Effects of Material Non-linearity on the Structural Performance of Sandwich Beams made of Recycled PET Foam Core and PET Fiber Composite Facings: Experimental and Analytical Studies

Raghad Kassab and Pedram Sadeghian[1]

Department of Civil and Resource Engineering, Dalhousie University, 1360 Barrington Street, Halifax, NS, B3H 4R2 Canada

ABSTRACT: This paper presents the results of experimental and analytical studies on sandwich beams subjected to three-point bending beyond their limit of proportionality. The sandwich beams were composed of polyethylene terephthalate (PET) fiber-reinforced polymer (FRP) composite facings and recycled PET (R-PET) foam core made from post-consumer plastic bottles. The study tested three R-PET core densities (70, 80, and 100 kg/m^3) and compared the results to a control group with 100 kg/m^3 core density and glass FRP facings. The beam geometry and testing set-up were consistent throughout the study, with 12 beams tested in total. The results showed that all specimens exhibited non-linear load-deflection behavior, resulting in developing a non-linear analytical model using decreasing secant elastic and shear moduli under increasing loads. The proposed model was validated, and a parametric analysis was performed to evaluate its mechanical performance under different conditions, including variations in span length and the thickness of the core and facing components. Additionally, the study created a novel failure mode map to predict the failure mechanism of the sandwich panels based on core density and the PET FRP facing thickness to span length ratio, considering the non-linear behavior of both components. As

[1] Corresponding author: Pedram Sadeghian, Associate Professor and Canada Research Chair in Sustainable Infrastructure, Department of Civil and Resource Engineering, Dalhousie University, Halifax, NS, Canada. Email: Pedram.sadeghian@dal.ca

a result, this study provides valuable insights into using recycled materials in construction, contributing to reducing plastic waste and mitigating environmental impact.

Keywords: Sandwich composite; PET; Recycling; Non-linear; Modeling; Test.

DOI: https://doi.org/10.1016/j.istruc.2023.05.119

1. INTRODUCTION

Plastic waste pollution continues to inspire global news headlines covered by environmental campaigners and activists [1, 2]. Over time, the public's perception of plastic has transformed from being considered a miracle to a curse [3]. Despite plastic's superior properties, inexpensive production costs [4, 5], and significant contribution to the world's economy [6], poor waste management techniques have overshadowed the advantages [7], and the public has waged war on plastic and essential plastic products. However, the issue with boycotting plastic products concerns how plastic alternatives–in many cases–have a more significant negative impact on the environment [8]. A practical approach for handling the ongoing dilemma is to enhance the plastic waste management sector and upcycle the waste to more value-added products with the larger market, such as construction sectors.

Mechanically recycled plastic is often met with resistance from industrial sectors, particularly the food packaging industry, which primarily uses virgin plastic due to concerns over contamination and potentially toxic substances leaching into food [9, 10]. In light of these concerns, it may be more appropriate to recycle plastic in a less sensitive industry, such as construction. There has been extensive research on recycling polyethylene terephthalate (PET) plastic in concrete mixes [11-20]. PET is a commonly used form of plastic in items such as single-use food containers, water and carbonated drink bottles, and prescription vials. The use of recycled

PET aggregate and fibers in concrete represents progress in plastic waste management, but the amount consumed during this application is a small fraction of the overall volume and has a limited impact on the plastic waste problem. Furthermore, as the percentage of recycled PET increases in the concrete mix, the compressive strength and stiffness decrease [11-20], highlighting the need for more effective methods of recycling PET waste in the construction industry.

In recent years, the construction industry has seen a surge in interest in fiber-reinforced polymer (FRP) and sandwich composites made from sustainable materials. Sandwich panels offer high structural efficiency, making them ideal for utilizing a diverse range of materials, including recycled and renewable materials. Despite this potential, most sandwich panels used for engineering applications are still made from non-recycled materials. To address this issue, researchers are exploring ways to create more sustainable sandwich panels using eco-friendly materials [21-32].

The exploration of the use of Polyethylene Terephthalate (PET) fibers in Fiber-Reinforced Polymer (FRP) composites is in its early stages. The benefits of using PET include its large capacity for rupture, low production cost, and potential for being derived from PET waste [33-35]. However, PET FRP has a lower modulus of elasticity compared to traditionally used fibers, such as glass, aramid, and carbon [33, 36]. This drawback can be mitigated by adding additional layers of PET FRP [33]. So far, the primary application for PET FRP has been for confining concrete columns. Consequently, much of the research in this area focuses on changing various parameters, such as PET FRP's geometry and testing mechanism, on establishing design guidelines for this specific use. Previous studies have analyzed the performance of reinforced concrete, plain concrete, and concrete-filled steel columns confined with PET FRP under axial compression [33-44]. The results have shown that PET FRP-confined concrete columns exhibit superior strength

and ultimate strain efficiency compared to those confined with Carbon FRP (CFRP) or Glass FRP (GFRP) [34]. Additionally, PET FRP has been reported to increase the shear capacity of reinforced concrete beams [36] and the lateral ductility of concrete columns [37]. Overall, the use of PET FRP in concrete confinement continues to show promise.

On the other hand, PET foam has received added attention in the sandwich panel industry analogous to that gained by PET fibers in the FRP sector; PET foam is the latest form of foam to be recognized as a core material used for structural sandwich panels [46]. Despite its recent acknowledgement [47], PET foam's advantages—including its recyclability, lightweight quality, relatively high mechanical properties (compared to PU foams) [48], and fatigue resistance [47]—have inspired numerous researchers to analyze sandwich panels with PET foam core. Shear response [49] and flexural behavior [50] of sandwich panels made from PET foam—subjected to elevated temperatures—were analyzed in recent literature. Additionally, numerical modeling was conducted to provide further details on the creep response, which is primarily beneficial when those panels require enduring long-term sustained loads [51]. To assess PET foam's practicality and use in a building's floor panels, the short- and long-term mechanical behaviors of panels made from PET cores and GFRP facing were analyzed.

Consequently, testing results concluded its adequacy for the proposed application [50]. As illustrated above, existing investigations remain focused on using virgin PET foam rather than recycled foam material. The market of recycled structural PET foam—created after concerns surrounding plastic waste pollution—is fairly new, limiting its availability to researchers. Therefore, previous studies lack analysis of recycled structural PET foam while focusing on foam obtained from virgin material. From an environmental perspective and considering its life cycle assessment (LCA), recycled PET (R-PET) foam is superior to virgin PET, along with all types of

traditionally used structural foams: polyurethane (PU), polyvinyl chloride (PVC), styrene acrylonitrile (SAN), and extruded polystyrene (XPS). This is owed to the recycled foam's lower carbon footprint, abiotic depletion, acidification, eutrophication, and photochemical smog. Hence, replacing conventional foam with recycled PET foam could potentially increase the sustainability of a given product and significantly reduce carbon emissions—which contributes to global warming—when used as a replacement to foams that are currently and vastly used for sandwich panels in the construction industry [52].

This study aims to fill the existing knowledge gap in the utilization of R-PET plastic waste as the core material in sandwich beams. The core component constitutes the bulk volume of the sandwich beam, and thus, incorporating waste plastic in the core instead of the facing results in a substantial waste reduction. The facing component was made from PET FRP composite sheets, using virgin PET fibers due to the limited availability of recycled PET fabric. Future studies could investigate the post-recycling performance by utilizing recycled PET fibers. The study will encompass the evaluation of the PET FRP composite under uniaxial tension, the R-PET core via shear testing, and the sandwich beams through three-point bending. Analytical models were established to verify the experimental findings, and a parametric study was performed to examine the effect of changing complex parameters that were not evaluated during experimental testing.

2. EXPERIMENTAL PROGRAM

The experimental program evaluated sandwich beam sets under identical flexural loading conditions to assess and compare their mechanical properties and bending performance. The mechanical properties of the facing and core components were obtained prior to testing the beams in bending. This section describes the fabrication process of the sandwich panels; the geometry of

the beam specimens; changing variables among the beam sets; the test set-up; and the method by which data was processed during testing.

2.1 Test Matrix

Table 1 illustrates the test matrix of 12 sandwich beams tested in this study. The sandwich beam specimens were divided into four sets, each encompassing three identical specimens with a length of 1200 mm, a width of 76 mm, and a total height of 82 mm. The two changing parameters among sets included the material type used for the facing component and the density of the core component. The core component was made from R-PET foam with a density ranging from 70 to 100 kg/m^3; the facing component was made from either 3 mm thick GFRP or PET FRP sheets, depending on the sandwich set. All other parameters—including testing method, dimensions of sandwich beams, and unsupported span length—were constant throughout testing. The specimens were identified based on the changing parameters considered during the study and their order within each set. The specimen's ID consists of three parts, each separated by a hyphen. The first corresponds to the type of FRP used for the facing component; the second corresponds to the type and density of the core material; and the third contains the number distinguishing the specimen in a particular set.

2.2 Material Properties

The sandwich specimens' facing component was constructed using PET FRP, with a polymer matrix reinforced by fibers. The polymer matrix, consisting of West System 105 (resin) and West System 206 (hardener), was mixed at a 5:1 volume ratio as advised by manufacturer Gougeon Brothers Inc. The PET fibers weighed 1742 g/m^2, had a tensile strength of 0.74 GPa, and an elastic modulus of 10 GPa. The glass fibers used in the GFRP were sourced from Haining Anjie

Composite Material Ltd and weighed 900 g/m^2, had a tensile strength of 1.5 GPa, and an elastic modulus of 72 GPa.

The mechanical properties of the sandwich specimens' facing components were obtained through coupon testing. Three coupons from each FRP set were fabricated using a wet lay-up process, consistent with the method for fabricating the sandwich panels and tested in uniaxial tension per ASTM D3039 [54]. The testing results provided the stress-strain response of GFRP and PET FRP coupons as shown in Figure 1. Under uniaxial tension, GFRP coupons possessed a linear stress-strain response with an average elastic modulus of 25692 ± 2433; and an average ultimate stress (f_u) and ultimate strain (ε_u) of 391±5 and 0.0152±0.0011, respectively. As shown in Figure 1, the PET FRP stress-strain relation was non-linear and thus deemed bilinear consisting of two straight lines intersecting at the yielding point. The first line corresponds to the stress-strain relation within the elastic zone; the second corresponds to the plastic zone. The average elastic (E_1) and plastic (E_p) moduli were found to be 7410±1884 and 3111±358, respectively. The average yielding (f_y) and ultimate stresses (f_u) were equivalent to 73±5 and 281±5, respectively. The average yielding strain (ε_y) and ultimate strain (ε_u) were 0.0118±0.0023 and 0.0911±0.001, respectively. Comparing the two types of FRPs used in the facing components of sandwich beams, PET FRP has four times the strain capacity and 25% less ultimate strength capacity compared to GFRP.

Consequently, GFRP is considerably stiffer, with an elastic modulus three times that of PET FRP. Based on the stress-strain data obtained through a uniaxial test, a new model was developed for the PET FRP composite using the Richard-Abbott equation [53]. The degree of curvature of the transition section between the elastic and plastic zones of the bilinear stress-strain response is described by the shape parameter "n." The location of the transition zone is specified

based on the reference plastic stress "f_o": the y-intercept of the second slope of the bilinear curve. The developed model illustrated in Equation (1) outputs stress with respect to strain at any location along the stress-strain bilinear curve. Due to the significant strain capacity of PET FRP, the strain response is difficult to accurately measure beyond the yielding point using conventional strain monitoring devices (e.g., strain gauges, extensometer). Consequently, mathematical relations linked terms prior to and past the yielding zones together to provide an approximate estimation of the shape parameter, reference plastic stress, and plastic modulus values. This model was used to account for the facing component's non-linearity while developing the sandwich beam's load-deflection model under three-point bending.

$$f = \frac{(E_1 - E_p)\cdot\varepsilon}{\left(1+\left|\frac{(E_1 - E_p)\cdot\varepsilon}{f_o}\right|^n\right)^{1/n}} + E_p \cdot \varepsilon \quad (1)$$

Based on data acquired from the PET FRP coupon's uniaxial tension test, the terms past the elastic stress-strain region are estimated as follows; $n = 3$, $E_p = E_1/3$, and $f_o = 2f_y/3$. The experimentally acquired stress-strain curve was first plotted along with the bilinear model. Then, the terms were approximated such that the bilinear model was comparable with the experimentally derived stress-strain curve, as shown in Figure 1.

The foam core is derived entirely from recycled post-consumer plastic bottles through a patented manufacturing method. This method transfers the waste bottles into clean granules extruded into continuous foam boards using a foaming agent. Depending on the intended application, the foam boards are cut and welded into specific dimensions to meet consumer demand. The mechanical properties of this product were acquired by the manufacturer (Armacell, Capellen, Luxembourg) through a series of controlled tests performed following standard guidelines specified for foam testing. The shear stress-strain relationship of R-PET foam was not

listed as part of the mechanical properties; however, previous research focused on experimental evaluation of virgin PET foam demonstrated that its shear stress-strain relationship is non-linear [49, 55]. This implies that R-PET foam would also exhibit non-linear mechanical behavior under shear.

Table 2 compares the mechanical properties of R-PET used in this study and those of PET foams (non-recycled), with data for the latter sourced from the product datasheet provided by a manufacturer [56]. The shear strength and modulus values for the R-PET foam, reported by the manufacturer, align closely with those of PET foam. For a foam density of 70 kg/m^3, the shear modulus for R-PET stands at 13 MPa, with a shear strength of 0.5 MPa. In comparison, PET foam at a marginally lower foam density of 65 kg/m^3, presents a shear modulus of 14 MPa and shear strength of 0.55 MPa. The minor 7.7% and 10% differences in these values exist despite PET's 7.1% lower density. At 80 kg/m^3, R-PET matches PET foam's shear modulus and only exhibits a slight decrease in shear strength. At the highest density of 100 kg/m^3, R-PET's values are about 9.5% and 20% lower than those of PET foam. Nonetheless, these values, validated under ISO 1922 standards, remain within the acceptable range for their use as structural foam in sandwich beams. Thus, despite minor disparities, the shear mechanical properties of R-PET foam are close to those of PET foam, reinforcing R-PET's potential as an eco-conscious alternative that supports a circular economy and reduces dependence on raw materials.

In addition to the ultimate shear strength and elastic modulus of R-PET foam—provided by the manufacturer—it is essential to acquire its complete shear-stress strain relation. This is critical since R-PET holds a non-linear shear stress-strain trend. Therefore, the modulus of elasticity is not constant throughout the curve; instead, the modulus will depend on the distinct value of the shear stress and strain reached under loading. R-PET foams with densities of 70 kg/m^3,

80 kg/m^3 and 100 kg/m^3 were tested under shear following ASTM C273 standards. Three foam specimens were tested from each density. Figure 2 (a) illustrates the shear fixture used in the testing process. As shown in Figure 2 (b), Instron 8501 was used to load the steel plates at a displacement control rate of 0.5 mm/minute. The load was subsequently transferred from the steel plate to the foam specimens through the glue connection between the two surfaces. The shear test was carried out until each specimen reached its peak load. The test results were only considered for specimens that had undergone diagonal tension shear failure occurring along the length of the specimens, as shown in Figure 2 (c). This implied excluding testing results of specimens exhibiting bond failure or other forms of premature failure modes. Figure 3 presents the shear stress-strain results of the tested specimens. As shown in the graph, the ultimate shear strength and initial shear modulus values are approximately equivalent to the values reported by the manufacturer in Table 2. In addition, the curves from Figure 3 demonstrate that the stress-strain relation of R-PET foam could be broken down into two linear sections. The bilinear stress-strain relation stems from the thermoplastic aspect of the R-PET foam; therefore, this trend is evident in all the tested foam specimens despite the change in foam densities among them. As the R-PET density increased from 70 kg/m^3 to 100 kg/m^3, this contributed to an increase in the initial shear modulus of the tested foam samples. The change in shear modulus occurred at different stress and strain values for each foam density. However, the second shear modulus was approximately 1.4 MPa and was constant for all the tested foam types. Richard-Abbott Equation was utilized to account for the bilinear trend of R-PET foams' shear stress-strain relation within the load-deflection model of the sandwich beams. The input terms of the Richard-Abbot Equation were unique for every foam type. Table 3 lists the input parameters associated with each type of R-PET foam. The bilinear shear stress-strain

model of the R-PET foam was plotted along with the shear test output in the graph presented in Figure 3.

Furthermore, the R-PET foam was experimentally tested to obtain its compressive stress-strain behavior in accordance with the ASTM C365-03 standard method for evaluating the compressive properties of sandwich core materials. The experiments involved subjecting five cuboid specimens of varying densities, as depicted in Figure 4, to a compressive load at a displacement rate of 2 mm/min for 15 minutes. Each specimen had a cross-sectional length and width of 70mm and a thickness of 50mm. The deformation of the specimen under increasing load was closely monitored using a combination of two techniques: digital image correlation (DIC) and laser extensometer. This was achieved by applying a patterned paint spray on one side of the cuboid for the DIC technique while attaching two reflective tapes on the other side of the specimen as part of the laser extensometer set-up, as depicted in Figure 5.

Deformation of the foam coupons was collected at a rate of 10 data points per minute using both the DIC and laser extensometer techniques. The camera used for the DIC technique had the capacity to capture 20 frames per minute. The distance between the two reflective tapes on the cuboid was measured before the test. This measurement was used during data processing of the laser extensometer reading to determine the change in the cuboid's vertical strain under compression. The results of the experimental study demonstrated that all R-PET foam samples tested had a linear correlation between the applied compression stress and the produced strain at the beginning. This linear correlation was then followed by a plateau phase, in which the foam began to show yielding. After this stage, the foam specimens progressed into a strain-hardening region until the end of the test.

The deformation readings obtained from the laser extensometer were found to be inaccurate during the initial linear deformation stage. However, the precision of the laser extensometer readings improved as the samples reached the yielding point. In contrast, the DIC technique provided consistent and accurate results throughout the initial deformation stage and up to approximately the midpoint of the yielding region. Therefore, the initial stress and strain response values of the foam under compression were determined using the deformation readings obtained from the DIC technique. In contrast, the laser extensometer was used to obtain the stress-strain response after the initial yielding zone. Figure 6 demonstrates the compression stress-strain curve obtained from the tested foam coupons. The initial stage of the stress-strain relationship is indicative of the foam's elastic behavior prior to the failure of its cell walls. The modulus of elasticity, an indicator of the foam's elastic resistance to deformation, was approximately 40 MPa, 50 MPa and 70 MPa for foam samples with densities of 70 kg/m^3, 80 kg/m^3 and 100 kg/m^3, respectively. The average yield stress, at which the linear elastic relationship between stress and strain in foam transforms into a prolonged plateau phase due to foam densification, is -0.02 MPa for all foam densities. As illustrated in Figure 6, the compression stress-strain relation displays a smooth transition from the prolonged densification phase into a strain-hardening phase, which persists until the conclusion of the test. The vertical lines appearing in the final phase of the relation are a result of the laser extensometer's inability to measure the change in deformation as the distance between the reflective tapes becomes undetectable.

2.3 Specimen Fabrication

Initially, sandwich panels with a width of 300 mm and length of 1200 mm were fabricated following a wet lay-up method, and then the panels were cut into 76 mm wide and 1200 mm long beams specimens. The core thickness was also 76 mm for all specimens. Figure 7 (a-e) illustrates

the fabrication process where the first facing component was created and glued to the foam core; the first unidirectional fabric layer was cut to the required length and traced onto parchment paper. Next, a layer of two-part epoxy resin was spread evenly within the traced section. The fabric was then placed on top of the resin layer, and another layer was applied to the stitched sheet of fabric. Finally, the core component was placed on top of the resin layer, while the first side was cured for four days. The transverse lines appearing in Figure 7 (e) result from welding the extruded foam product together during the manufacturing process. The second side of the sandwich panel was created following the same procedure. Once fully cured, the panel was cut into four equal beam sections of 76x82x1200 mm, as shown in Figure 7 (f). All sets of sandwich panels were fabricated following the same procedure. The unidirectional glass fabric was five times thinner compared to the unidirectional PET fabric. Therefore, five layers of glass fabric were used while fabricating each facing component of a GFRP-faced sandwich panel set. The facing components of the sandwich panels were approximately 3 mm thick, as outlined in Table 1.

2.4 Test Set-Up and Instrumentation

Three-point bending tests were performed on sandwich specimens using the set-up illustrated in Figure 8. The beams were supported on two steel rollers (1100 mm span) with an overhang distance of 50 mm on each end. A concentric load was applied through a hollow structural section (HSS) at a displacement-controlled rate of 6 mm per minute. Two strain gauges were mounted on the top and bottom facing of the sandwich at midspan length. This captured the tension and compression strains, and a string potentiometer was attached at midspan length to identify the maximum displacement of the beam during bending. The load cell, string potentiometer, and strain gauges were connected to a data acquisition (DAQ) unit, which was set to collect and record ten data points per second. All sandwich beams were loaded until failure; thus, the test was terminated

once the beams reached ultimate strength capacity. Two cameras were used to record each test and help identify the mode at which the sandwich failed.

3. EXPERIMENTAL RESULTS AND DISCUSSION

Table 4 summarizes the test results at peak load. The results show that the failure load also increases as the foam core density increases from 70 kg/m^3 to 80 kg/m^3. However, when the foam core density increases from 80 kg/m^3 to 100 kg/m^3, the peak load reached by the sandwich beams no longer increases. All other material properties were considerably more influenced by the change in the facing component than the change in core density. Additionally, sandwich specimens made from GFRP facing had significantly higher stiffness and strength compared to specimens made from PET FRP facings. This is because the facing component resists bending forces, and the PET FRP composite has a lower modulus compared to GFRP. The compression strain gauge of one of the specimens (GFRP-R-PET100-1) made from GFRP facing and foam core set failed during the test; thus, this specimen's compression strain was not considered or reported for this study. The following subsections will present further analysis regarding the mechanical performance of each different sandwich beam set based on data captured throughout the testing interval.

3.1 Load-deflection Behavior

The total deflection in sandwich beams under concentric load combines bending and shear deflection. The impact of shear deflection on a total deflection in monolithic beams is minimal. In the case of composite sandwich beams, however, the presence of components with varying mechanical properties can significantly affect the total deflection, mainly when the core exhibits a lower shear modulus than the components forming the facings, as evidenced in the current study. The shear stress-strain relationship of thermoplastic foam is non-linear, leading to a non-linear

load-deflection relationship for beams loaded in three-point bending. The total deflection was measured and recorded using a string potentiometer during experimental testing, yielding the deflection curves discussed in this section. A comprehensive analysis of the breakdown of the total deflection will be presented in a subsequent section of this study.

The load-deflection curves of all tested sandwich beams were deemed non-linear. Evidently, non-linearity stems from the recycled PET core and the PET FRP facing. Generally, the stiffness of the sandwich beam's facing component directly influences the overall beam's stiffness. This was observed in the load-deflection curve presented in Figure 9; the sandwich beam set comprised of stiffer facing (e.g., GFRP) had a higher stiffness capacity compared to beams made from a less stiff facing material (e.g. PET FRP). As expected, the core component's density had a minor influence on the overall stiffness of the beam. As the density of the sandwich beam's core increased from 70 kg/m^3 to 80 kg/m^3, its stiffness subsequently increased, as shown in Table 4.

3.2 Load-strain Behavior

In a three-point bending load configuration, the sandwich beams undergo bending deflection that results in compression on the top facing and tension on the bottom facing. Results from Figure 10 indicate that sandwich beams with PET FRP facings have a superior strain capacity compared to those with GFRP facings. The sandwich beam's failure mode is defined by face wrinkling, not face rupture. This means the facing component does not reach its maximum strain capacity at peak load. Figure 10 displays the linear load-strain behavior of sandwich beams with PET FRP facings during the initial bending stage, which has not yet reached the yielding point shown in Figure 1. The load-strain curve becomes non-linear when the facing component reaches its yielding strain. On the other hand, sandwich beams with GFRP facings exhibit a linear load-strain relationship

due to the linear stress-strain correlation of the GFRP material. Additionally, Figure 10 shows how the strain of the PET FRP depends on the orientation of the applied force, resulting in maximum strains of approximately 15,000 με and 10,000 με for the compression and tension faces, respectively, at the ultimate strength capacity of the sandwich beam.

3.3 Moment-curvature Behavior

Figure 11 presents the moment-curvature relationship for each set of beams. The moment-curvature relation is mostly influenced by the mechanical properties of the facing component, producing two groups of curves - one for sandwich beams with PET FRP facings and one for those with GFRP facings. Sandwich beams with PET FRP facings exhibit higher curvature at a given moment due to the greater strain capacity of the PET FRP composite. In contrast, sandwich beams with GFRP facings have greater moment resistance owing to the higher strength capacity of the GFRP composite.

3.5 Failure Mode

Sandwich beams commonly fail through three main modes: core shear (CS), face yield/rupture (FY/FR), and top face wrinkling (FW). When a failure load initiates a particular mode, other modes can follow in rapid succession. This was observed during testing, where face wrinkling caused the beam's failure, followed by immediate shearing of the foam core, as seen in Figure 12, a video snapshot captured during testing and analyzed in slow motion. Figure 13 shows all sandwich beams after reaching their ultimate strength in three-point bending. As noted in Table 4, all beams failed through face wrinkling, except for one specimen made of PET FRP facing and R-PET foam core with a density of 80 kg/m^3, which failed through compression face rupture.

4. ANALYTICAL STUDY

The study analyzed the mid-span deflection response of sandwich beams when subjected to concentric loads. The deflection was determined by considering the combined effect of bending and shear deflections, each of which was modeled individually. The analytical models were used to verify the experimental testing results and provide a deeper understanding of the deflection behavior. Furthermore, a parametric study was conducted to examine the influence of varying geometric parameters of the sandwich beams on the deflection response, providing valuable insights into the design and optimization of sandwich structures.

4.1 Scope

As described in Section 2.2, the non-linearity of the sandwich beam's facing component was illustrated through the uniaxial tension test, while data obtained through shear and compressive tests on R-PET foam coupons indicated the non-linearity of the core component. In addition, the experimental investigation on the sandwich beam specimens concludes that the material non-linearity of the core and facing components affects the mechanical behavior of the overall beams under three-point bending. Thus, it is necessary to account for the non-linearity of the sandwich beams facing and core components within the analytical model.

Several analytical methods have been used in recent studies to account for the described non-linearity. Fu and Sadeghian [57] accounted for the material non-linearity by assuming that the normal stress-strain relationship of the facing component and the shear stress-strain relationship of the core component follows a parabolic trend. Betts et al. [21] developed similar models based on experimentally acquired non-linear stress-strain data of the facing component. More complex models have been developed using finite element analysis software [58]. In this study, the

analytical model was developed following an iterative procedure comprised of the Richard-Abbott equation to account for the material non-linearity of the facing and core components. Furthermore, a novel approach was used to account for the bilinear stress-strain relationship within the failure mode map in which two sets of transition lines were developed using two distinct elastic moduli.

4.2 Non-linearity of Bending Deformation

The non-linear normal stress-strain correlation of the sandwich beam's facing component causes a non-linearity in bending deflection. Since PET FRP demonstrates such non-linearity—which is presented in the previous experimental section—sandwich beams made from PET FRP facings will undergo non-linear bending deformation once the yielding stress of the facing component is reached under the concentrically applied load. In contrast, sandwich beams made from GFRP facing will not experience non-linear bending deformation since GFRP possesses a linear stress-strain relationship under uniaxial tension. Hence, the non-linear bending deformation model is exclusively dedicated to sandwich panels made from PET FRP facings.

The flowchart presented in Figure 14 illustrates, in sequence, the process of obtaining bending deflection at each load step until the maximum deflection is reached. As described in the flowchart, the beam's geometric aspects (e.g. length: L; width: b; distance between facing's centroid: d; moment of inertia: I; and thickness of facing component: t_f), facing component's mechanical properties (e.g. elastic modulus: E_1; plastic modulus: E_p; shape parameter: ν; and reference plastic stress: σ_o), and initial: P_o; ultimate loads: P_f; and loading increments: ΔP were first inputted as constants. The load was then converted into moment, M, which was used to calculate the stress resisted by the facing component, σ_f, through the following equations:

$$M = \frac{P_i L}{4} \tag{2}$$

$$\sigma_f = \frac{M}{b d t_f} \tag{3}$$

Consequently, the strain was derived from the value of stress using the Richard-Abbott equation, thus accounting for the material non-linearity of PET FRP. Since Richard-Abbott's Equation cannot be algebraically rearranged to yield strain in terms of stress, "GoalSeek"—Excel's built-in analysis tool—was used to output strain values. The secant modulus was calculated using the stress and strain values associated with a specific load step. Subsequently, the bending deflection was derived as follows:

$$E_{sec} = \frac{\sigma_f}{\varepsilon} \tag{4}$$

$$(\delta_b)_i = \frac{P_i L^3}{48\, E_{sec}\, I} \tag{5}$$

This procedure was repeated for every load step until the deflection—due to the ultimate applied load—was calculated.

4.3 Non-linearity of Shear Deformation

The deflection caused by shear stress is significantly smaller than bending deflection for monolithic beams and, therefore, often excluded within the total deflection calculation. In contrast, sandwich beams' shear deformation is significant with respect to their total deflection and hence should be considered through the calculation. As the distance between a beam's supports decreases and/or the difference between a sandwich beam's core shear modulus and facing elastic modulus increases, the magnitude of shear deflection and the ratio of shear deflection to total deflection increase, accordingly. Consequently, shear deflection was accounted for while modeling the total deflection of all beam sets. The effect of material non-linearity of R-PET foam was observed during experimental testing and was considered within the shear deflection model.

As shown in the flowchart of Figure 15, the inputs of the shear deflection model include initial load, final load, loading increments, beam width, moment of inertia, and its unsupported span length during testing. Additionally, the thickness of the facing component, the distance

between the facing's centroid, the core component's initial shear modulus, G_1, plastic shear modulus, G_p, reference plastic shear stress, τ_o, and ultimate shear strength, τ_u. As Figure 3 illustrates, Richard-Abbott equation was deemed viable in predicting the response of R-PET foam. Therefore, it was utilized—as shown in Equation (6)–within the non-linear model of shear deflection.

$$\tau = \frac{(G_1 - G_p)\,\gamma}{\left\{1+\left[\frac{(G_1 - G_p)\gamma}{\tau_o}\right]^n\right\}^{\frac{1}{n}}} + \gamma G_p \tag{6}$$

The initial shear deflection—resulting from the first load step—was obtained by applying the constant inputs into the shear deflection equation as follows:

$$(\delta_s)_i = \frac{P_i L}{4 G_c b d} \tag{7}$$

As represented in Equation (8), the value of initial shear deflection was used to obtain the secant shear modulus, G_s, which derived the shear deflection corresponding to the subsequent load step.

$$(G_s)_i = \frac{(G_1 - G_p)}{\left\{1+\left[\frac{2(G_1 - G_p)\delta_s}{L\tau_o}\right]^n\right\}^{\frac{1}{n}}} + G_p \tag{8}$$

This process was repeated to account for the material non-linearity of R-PET foam until the maximum shear displacement at ultimate load was calculated.

4.4 Verification of Load-Deflection Model

The total midspan load-deflection models—the sum of bending and shear deflection models—of the four beam sets were compared to the load-deflection curves obtained through experimental testing, as shown in Figure 16 (a-d). The total midspan load-deflection models derived through the iterative processes outlined in the previous section, which involved using variable secant modulus for each load step, are labelled as "non-linear" models. "Linear" models were obtained using a

constant core shear modulus and facing elastic modulus; hence, those models do not account for the material non-linearity of the facing and core components. Linear models most accurately predict midspan deflection at the initial loading stage since the material non-linearity of R-PET foam and PET FRP have not yet been developed. Shortly afterwards, however, the linear model becomes increasingly less accurate, and the non-linear model becomes gradually more accurate in predicting the load-deflection trend.

4.5 Contribution of Shear and Bending Deflections to Total Deflection

The source of deflection was investigated while analyzing the total deflection response of the sandwich beams. Upon exerting a load at the midpoint of the sandwich beam, a deflection response is initiated. The total deflection at this midspan, symbolized as δ_t, is a cumulative result of two components: the deflection instigated by bending, δ_b, and the one prompted by shear, δ_s. The total midspan deflection under the influence of the load is obtained through the following equation:

$$\delta_t = \delta_b + \delta_s = \frac{PL^3}{48(EI)_{eq}} + \frac{PL}{4(AG)_{eq}} \quad (9)$$

In which, the term $(EI)_{eq}$ denotes the equivalent flexural rigidity, which is a measure of the beam's resistance to bending under the applied load. The variable P denotes the applied load, referring to the external force placed upon the midpoint of the sandwich beam. The term $(AG)_{eq}$ is the equivalent shear rigidity, representing the beam's resistance to deformation from a force applied in parallel to its length, and the term L corresponds to the unsupported span length [59].

As shown in Figure 17 (a-d), the total midspan deflection of the four types of sandwich beams was broken down into shear and bending deflections. The increase in R-PET foam density resulted in a decrease in the contribution of the bending deflection to total deflection. Furthermore, Figure 17 (a-d) reveals that as the facing component shifts from PET FRP to GFRP, the contribution of shear

deflection surpasses that of bending deflection to the overall deflection. Therefore, as the sandwich beam's facing or core component's stiffness increases, the relative contribution of bending deflection to the total deflection decreases correspondingly.

4.6 Effect of Non-linearity of PET FRP on Failure Mode Map

A failure mode map was developed to predict the failure mechanism of any sandwich beam made from PET FRP facing and R-PET foam—loaded in a three-point bending configuration—based on the density of the core component and the ratio of the facing component's thickness to unsupported span length. An experimental investigation was carried out to determine the mechanical properties of the core component, including shear strength, shear modulus, and compressive elastic modulus, at multiple densities. The methodology employed and comprehensive results of this study are documented in detail in the preceding section. The acquired data was then plotted, as shown in Figure 18(a-d), and the functions relating the mechanical properties of R-PET foam to its density were derived accordingly. The map considers three modes of failure: face rupture, core shear, and face wrinkling. Standard failure mode maps primarily involve sandwich beams with a facing component that has a single modulus of elasticity (e.g., steel, aluminum, and GFRP); hence, one set of transition lines is used to outline the border of each failure mode zone. Since PET FRP's stress-strain correlation was deemed bilinear, both initial, E_1, and ultimate secant moduli, E_{su}, were used while constructing the failure mode map. Therefore, as shown in Figure 19, two sets of transitions were constructed, each considering a different modulus.

4.7 Parametric Study

After verifying the developed models, a parametric study was conducted on sandwich beams made from PET FRP facing and R-PET foam core density of 80kg/m^3, 200 kg/m^3 and 320 kg/m^3. The study critically analyzed the mechanical performance of the sandwich beams regarding additional

parameters not considered within the experimental analysis. Through the parametric study, unsupported span length, the thickness of the core component, and the facing components were analyzed at a range between 3m to 6m, 3mm to 12mm, and 75mm to 150mm, respectively. While analyzing each parameter, the other two geometric aspects retained consistency; the unsupported span length was set to 3m, and the thicknesses of the core and facing components were set to 150mm and 6mm, respectively.

Results obtained through analyzing the effect of changing the sandwich beam's core thickness are presented in Table 5 and Figure 20. Results presented in Table 5, Table 6, Figure 20 (b, d, f), and Figure 21 (b, d, f) indicate that as the thickness of the core component or facing component increases at the three analyzed densities (ρ_c = 80 kg/m^3, ρ_c = 200 kg/m^3 and ρ_c = 320 kg/m^3), both initial, K, and ultimate stiffnesses, K_u, of the sandwich beam increase. Hence, deflection under a given load decreases, and the value of peak load, P_u, increases. Additionally, as demonstrated in Table 5, Table 6, Figure 20 (a, c, e), and Figure 21 (a, c, e), at a given load, strain change of the sandwich beam's facing component decreases in correspondence with the increase in core and facing components' thickness. Conversely, as the unsupported span length increases, the overall stiffness of sandwich beams decreases and their strain capacity increases, as shown in Figure 22 and Table 7. Overall results imply that face wrinkling is the governing mode of failure for most analyzed beams.

5. CONCLUSIONS

This paper presented the results of an experimental and analytical study on sandwich beams made from recycled PET foam core and PET FRP facings. Experimental testing demonstrated that the beams' non-linear deflection under concentrically applied load was due to the material non-

linearity of both PET FRP and R-PET foam; hence, both sources of non-linearity were considered while developing the analytical model. The analytical model confirmed the results obtained through experimental testing and helped establish a parametric study. Primary outcomes concluded from the experimental testing results as well as the analytical models, are summarized below:

- PET FRP's stress-strain behaviour under uniaxial tension is non-linear and can be approximated by a bilinear function through the Richard-Abbott equation.
- Compared to the GFRP composite created from the same polymer matrix, the PET FRP composite has four times more strain capacity and 25% less stress capacity.
- The non-linear load-deflection behavior of thermoplastic sandwich panels stems from the thermoplastic core (R-PET foam) and facing components (PET FRP).
- The contribution of shear deflection to the total deflection—resulting from the applied load—decreases as the core density is increased.
- The immense strain capacity of PET FRP causes face wrinkling to become the governing failure mode for most tested and modeled sandwich beams.
- Suggestions for future research include replacing epoxy matrix and virgin PET fibers with thermoplastic resin and recycled PET fibers, studying the effect of dimension variation on strength parameters, and testing the R-PRT foam core to characterize its non-linear shear behavior.

6. REFERENCES

[1] A. L. Brooks, S. Wang, J. R. Jambeck, The Chinese import ban and its impact on global plastic paste trade, Science Advances 4 (6) (2018) 1-7

[2] S. Yahya, Comparative life cycle assessment of beverages packages in Palestine, Journal of Cleaner Production 131 (2016) 28-42

[3] J. Payne, P. Mckeown, M. D. Jones, A circular approach to plastic waste, Polymer Degradation and Stability 165 (2019) 170-181

[4] J. Derraik, The pollution of the marine environment by plastic debris: a review, Marine Pollution Bulletin 44 (2) (2002) 842-852

[5] T. Letcher, Introduction to plastic waste and recycling, In Plastic Waste and Recycling, Elsevier, (2020) 3-12.

[6] T. R. Walker, D. Xanthos, A call for Canada to move toward zero plastic waste by reducing and recycling, Resources, Conservation & Recycling 133 (2018) 1-2.

[7] R. Sharma, P. P. Bansal, Use of different forms of waste plastic in concrete – a review, Journal of Cleaner Production 112 (2016) 473-482

[8] H. Pilz, J. Schweighofer and E. Kletzer, The Contribution of Plastic Products to Resource Efficiency, Gesellschaft fur umfassende Analysen, Vienna, 2005.

[9] US Food & Drugs Administration, 2018. [Online]. Available: <https://www.fda.gov/food/packaging-food-contact-substances-fcs/recycled-plastics-food-packaging>. [Accessed 14.04.20].

[10] Government of Canada, 2011. [Online]. Available: <https://www.canada.ca/en/health-canada/services/food-nutrition/legislation-guidelines/guidance-documents/guidelines-determining-acceptability-use-recycled-plastics-food-packaging-applications-1996.html>. [Accessed 14.04.20]

[11] R. Siddique, J. Khatib, K. Inderpreet, Use of recycled plastic in concrete: a review, Waste Management 28 (2008) 1835-1852

[12] B. Safi, M. Saidi, D. Aboutaleb, M. Maallem, The use of plastic waste as fine aggregate in the self-compacting mortars: effect on physical and mechanical properties, Construction and Building Materials 43 (2013) 436-442

[13] K. Hannawi, S. Kamali-Bernand, W. Prince, Physical and mechanical properties of mortars containing PET and PC, Waste Management 30 (2010) 2312-2320

[14] C. Albano, N. C. Camacho, M. Hernandez, A. Matheus, Influence of content particle size of waste pet bottles on concrete behaviour at different w/c ratio, Waste Management 29 (10) (2009) 2707-2716

[15] T. R. Naik, S. S. Singh, C. O. Huber, B. S. Brodersen, Use of post-consumer waste plastic in cement-based composites, Cement and Concrete Research 26 (10) (1996) 1489-1492

[16] N. Saikia, J. de Brito, Use of plastic waste as aggregate in cement mortar and concrete preparation: a review, Construction and Building Materials 34 (2012) 385-401

[17] S. Yang, X. Yue, X. Liu, Y. Tong, Properties of self-compacting lightweight concrete containing recycled plastic particles, Construction and Building Materials 84 (2015) 444-453

[18] A. Sadrmomtazia, S. Dolati-Milehsaraa, O. Lotfi-Omrana, A. Sadeghi-Nik, The combined effects of waste Polyethylene Terephthalate (PET) particles and pozzolanic materials on the properties of self-compacting concrete, Journal of Cleaner Production 112 (2016) 2363-2373

[19] L. Gu, T. Ozbakkaloglu, Use of recycled plastic in concrete: a critical review, Waste Management 51 (2016) 19-42

[20] M. A. Kamaruddin, M. M. A. Abdullah, M. H. Zawawi, M. R. R. A. Zainol, Potential use of plastic Waste as Construction Materials: Recent Progress and Future Prospect, IPO Science 267 (2017) 1-10

[21] D. J. Betts, P. Sadeghian, A. Fam, Structural Behavior of Sandwich Beams with Flax Fiber–Reinforced Polymer Faces and Cardboard Cores under Monotonic and Impact Loads, Journal of Architectural Engineering 26 (2) (2020)

[22] D. J. Betts, P. Sadeghian, A. Fam, Experimental Behavior and Design-Oriented Analysis of Sandwich Beams with Bio-Based Composite Facings and Foam Cores, Journal of Composites for Construction 22 (4) (2018)

[23] A. Mccracken, P. Sadeghian, Corrugated Cardboard Core Sandwich Beams with Bio-based Flax Fiber Composite Skins, Journal of Building Engineering 20 (2018) 114-122

[24] A. Mccracken, P. Sadeghian, Partial-Composite Behavior of Sandwich Beams Composed of Fiberglass Facesheets and Woven Fabric Core, Thin-Walled Structures 131 (2018) 805-815

[25] L. Aung, Fabrication of green sustainable sandwich panels by synthesis of polyurethane-based foams with incorporated "waste" glycol and agricultural "waste" residue, Ann Arbor: California State University (2014) 1-68

[26] P. R. Oliveira, A. M. S. Bonaccorsi, T. H. Panzera, A. L. Christoforo, F. Scarpa, Sustainable sandwich composite structures made from aluminium sheets and disposed bottle caps, Thin-Walled Structures 120 (2017) 38-45

[27] M. Hussain, N. Abbas, N. Zahra, U. Sajjad, M. B. Awan, Investigating the performance of GFRP/wood-based honeycomb sandwich panels for sustainable prefab building construction, Springer Nature Appl. Sci. 1 (2019)

[28] K. Shanmugam, S. Jansson, V. Gadhamshetty, L. Matsakas, U. Rova, M. Tysklind, P. Christakopoulos, V. K. K. Upadhyayula, Ecoefficiency of Thermal Insulation Sandwich Panels Based On Fly Ash Modified with Colloidal Mesoporous Silica, ACS Sustainable Chemistry & Engineering 7 (24) (2019)

[29] K. E. Chan, L. A. Yong, Y. Ko, S. Mendez, Experimental and numerical studies of sustainable sandwich bio-composites derived from plant-based resources, Journal of Sandwich Structures & Materials 19 (2) (2017) 192-215

[30] L. S. Rasheed, S. A. Ali, The Effect of the Shear Connectors Layout on the Sustainable Lightweight Concrete Sandwich, IOP Conference Series: Materials Science and Engineering 584 (2019) 1-10

[31] J. Susainathan, F. Eyma, E. D. Luycker, A. Cantarel, B. Castanie, Experimental investigation of impact behavior of wood-based sandwich structures, Composites Part A: Applied Science and Manufacturing 109 (2018) 10-19

[32] L. M. Chiacchiarelli, Sustainable, nanostructured, and bio-based polyurethanes for energy-efficient sandwich structures applied to the construction industry, Biomass, Biopolymer-Based Materials, and Bioenergy (2019) 135-160

[33] J. Dai, Y. Bai, J. G. Teng, Behavior and Modeling of Concrete Confined with FRP Composites of Large Deformability, Journal of Composites for Construction 15 (6) (2011) 963-973

[34] O. I. Abdelkarim, M. ElGawady, Concrete-Filled-Large Deformable FRP Tubular Columns under Axial Compressive Loading, Fibers 3 (2015) 1-18

[35] Y. Bai, J. Dai, J. G. Teng, Cyclic Compressive Behavior of Concrete Confined with Large Rupture Strain FRP Composites, Journal of Composites for Construction 18 (1) (2014)

[36] T. Jirawattanasomkul, J. Dai, D. Zhang, M. Senda, Experimental Study on Shear Behavior of Reinforced-Concrete Members Fully Wrapped with Large Rupture-Strain FRP Composites, Journal of Composites for Construction 18 (3) (2014)

[37] S. Saleem, A. Pimanmas, W. Rattanapitikon, Lateral response of PET FRP-confined concrete, Construction and Building Materials 159 (2018) 390-407

[38] A. Pimanmas, S. Saleem, Dilation Characteristics of PET FRP–Confined Concrete, Journal of Composites for Construction 22 (3) (2018)

[39] Y. Long, W. Lia, J. Daib, L. Gardner, Experimental study of concrete-filled CHS stub columns with inner FRP tubes, Thin-Walled Structures 122 (2018) 606-621

[40] T. Yu, S. Zhang, L. Huang, C. Chan, Compressive behavior of hybrid double-skin tubular columns with a large rupture strain FRP tube, Composite Structures 171 (2017) 10-18

[41] Y. Guo, S. Xiao, S. Shi, J. Zeng, W. Wang, H. Zhao, Axial compressive behavior of concrete-filled FRP-steel wire reinforced thermoplastics pipe hybrid columns, Composite Structures 244 (2020) 1-16

[42] Y. Bai, J. Dai, T. Ozbakkaloglu, Cyclic Stress-Strain Model Incorporating Buckling Effect for Steel Reinforcing Bars Embedded in FRP-Confined Concrete, Composite Structures 182 (2017)

[43] H. Naito, M. Akiyama, M. Suzuki, Ductility Evaluation of Concrete-Encased Steel Bridge Piers Subjected to Lateral Cyclic Loading, Journal of Bridge Engineering 16 (1) (2011)

[44] S. Saleem, Q. Hussain, A. Pimanmas, Compressive Behavior of PET FRP–Confined Circular, Square, and Rectangular Concrete Columns, Journal of Composites for Construction 21 (3) (2017)

[45] N. Pokharel, M. Mahendran, Experimental investigation and design ofsandwich panels subject to local bucklingeffects, Journal of Constructional Steel Research 59 (2003) 1533-1552

[46] Armacell, 2017. [Online]. Available: <http://www.armacell.us/products/armaform/?CA> [Accessed 23.04.20]

[47] K. A. Feichtinger, W. Ma, T. Touzot, Novel thermoplastic foam structural core material with enhanced thermoformability, fatigue endurance and elevated temperature properties, Semantic Scholar (2004)

[48] M. Garrido, J. R. Correia, Elastic and viscoelastic behaviour of sandwich panels with glass-fiber reinforced polymer faces and polyethene terephthalate foam core, Journal of Sandwich Structures & Materials 20 (4) (2018) 399-424

[49] M. Garrido, J. R. Correia, T. Keller, Effects of elevated temperature on the shear response of PET and PURfoams used in composite sandwich panels, Construction and Building 76 (2015) 150-157

[50] M. Rezaei, V. Karatzas, C. Berggreen, C. Berggreen, The effect of elevated temperature on the mechanical properties and failure modes of GFRP face sheets and PET foam cored sandwich beams, Journal of Sandwich Structures & Materials 22 (4) 1235-1255

[51] M. R. T. Arrudaa, M. Garrido, L. M. S. Castro, A. J. M. Ferreira, J. R. Correia, Numerical modelling of the creep behaviour of GFRP sandwich panels using the Carrera Unified Formulation and Composite Creep Modelling, Composite Structures 183 (2018) 103-113

[52] Armacell, 2015. [Online]. Available: <https://local.armacell.com/fileadmin/cms/pet-foams/Tech_Info/Tech_Info_LCA_.pdf> [Accessed 3.05.20]

[53] R. M. Richard, B. J. Abbott, Versatile elastic-plastic stress-strain formula, Journal of the Engineering Mechanics Division, Proceeding of the American Society of Civil Engineers 101 (1975) 511-515

[54] ASTM D3039. Standard Test Method for Tensile Properties of Polymer Matrix Composite Materials, West Conshohocken, PA, USA: ASTM International, 2008.

[55] L. Pyrzowski, B. Sobczyk, Local and global response of sandwich beams made of GFRP facings and PET foam core in three point bending test, Composite Structures 241 (2020)

[56] Airex, 2020. [Online]. Available: <https://www.3accorematerials.com/uploads/documents/TDS-AIREX-T10-E-04.2020.pdf> [Accessed 08.06.20]

[57] Y. Fu, P. Sadeghian, Flexural and shear characteristics of bio-based sandwich beams made of hollow and foam-filled paper honeycomb cores and flax fiber composite skins, Thin-Walled Structures 153 (2020)

[58] T. Sharaf, A. Fam, Numerical modelling of sandwich panels with soft core and different rib configurations, Journal of Reinforced Plastics and Composites 31(11) (2012)

[59] Zhang F, Xu J, Esther B, Lu H, Fang H, Liu W. Effect of shear span-to-depth ratio on the mechanical behavior of composite sandwich beams with GFRP ribs and balsa wood core materials. Thin-Walled Structures. 2020 Sep 1;154:106799.

Table 1. Test matrix of the sandwich beams

Set Number	Specimen ID	Facing Material	Facing Thickness (mm)	Total Thickness (mm)	Core Density (kg/m^3)	Number of Identical Specimens
1	PET FRP–R-PET70	PET FRP	3.0	82.0	70	3
2	PET FRP–R-PET80	PET FRP	3.0	82.0	80	3
3	PET FRP–R-PET100	PET FRP	3.0	82.0	100	3
4	GFRP–R-PET100	GFRP	2.7	81.4	100	3
Total						12

Note: Thickness and width of core component = 76 mm

Table 2. Mechanical properties of recycled PET (R-PET) foams used in this study compared with non-recycled PET foams obtained from the literature.

Foam Type	**R-PET**	**R-PET**	**R-PET**	**PET**	**PET**	**PET**
Density, ρ (kg/m^3)	70	80	100	65	80	100
Compression Modulus, E_c (MPa)	40	57	77	55	60	90
Shear Modulus, G_c (MPa)	13	16	21	14	16	23
Shear strength, τ_c (MPa)	0.50	0.60	0.75	0.55	0.65	0.9

Table 3 Input parameters of R-PET shear stress-strain model

Foam Density, ρ (kg/m3)	Elastic Modulus, G_1 (MPa)	Plastic Modulus, G_p (MPa)	Reference Plastic Stress, τ_o (MPa)
70	12.7	1.38	0.31
80	20.8	1.38	0.48
100	25.7	1.42	0.60

Table 4. Summary of test results

Specimen ID	Initial Stiffness (N/mm)	Load (kN)	Deflection (mm)	Tensile Strain (με)	Compression Strain (με)	Moment (N-m)	Curvature (1/m)	Failure Mode
PET FRP–R-PET70-1	106	3.73	42.8	9574	-9042	1043	0.22	FW→CS
PET FRP–R-PET70-2	107	3.48	37.2	8253	-12809	971	0.28	FW→CS
PET FRP–R-PET70-3	106	3.35	36.7	8144	-13303	936	0.28	FW→CS
PET FRP–R-PET80-1	124	4.05	37.6	8845	-13345	1132	0.27	FW→CS
PET FRP–R-PET80-2	127	4.58	43.5	9997	-14495	1280	0.31	FW→CS
PET FRP–R-PET80-3	120	4.18	41.7	10419	-14373	1167	0.30	FR
PET FRP–R-PET100-1	129	4.35	41.1	1083	-16606	1161	0.33	FW→CS
PET FRP–R-PET100-2	129	4.24	42.3	13345	-21967	1185	0.42	FW→CS
PET FRP–R-PET100-3	129	4.35	41.6	9776	-12156	1215	0.27	FW→CS
GFRP–R-PET100-1	250	7.30	41.7	5758	NA	2042	NA	FW→CS
GFRP–R-PET100-2	256	7.49	45.0	5803	-6881	2093	0.15	FW→CS
GFRP–R-PET100-3	263	7.17	38.8	3966	-7459	2004	0.14	FW→CS

Table 5. Results of parametric study on the effect of core thickness and core density (t_f = 6mm, L = 3m)

Core Thickness (mm)	**Core Density = 80 kg/m^3**							**Core Density = 200 kg/m^3**							**Core Density = 320 kg/m^3**						
	Initial Stiffness, K (N/mm)	Ultimate Stiffness, K_u (N/mm)	$\frac{K_u}{K_i}$	Peak Load, P_u (kN)	Def. at Peak, δ_u (mm)	Facing Strain at Peak, ε_u (μ ε)	Failure Mode	Initial Stiffness, K (N/mm)	Ultimate Stiffness, K_u (N/mm)	$\frac{K_u}{K_i}$	Peak Load, P_u (kN)	Def. at Peak, δ_u (mm)	Facing Strain at Peak, ε_u (μ ε)	Failure Mode	Initial Stiffness, K (N/mm)	Ultimate Stiffness, K_u (N/mm)	$\frac{K_u}{K_i}$	Peak Load, P_u (kN)	Def. at Peak, δ_u (mm)	Facing Strain at Peak, ε_u (μ ε)	Failure Mode
75	20.3	10.3	0.51	4.33	418	15300	FW	22.7	15.3	0.68	8.32	770	41000	FW	23.00	15.5	0.67	11.93	1238	66922	FW
100	33.7	15.7	0.47	5.67	361	15279	FW	38.6	26.1	0.68	10.77	590	40782	FW	39.29	26.5	0.67	15.62	951	66940	FW
125	49.7	20.8	0.42	7.01	337	15282	FW	58.6	39.7	0.68	13.31	480	40620	FW	59.89	40.3	0.67	19.30	772	66911	FW
150	68.26	26.9	0.39	8.34	310	15258	FW	82.5	56.1	0.68	15.85	405	40510	FW	84.70	57.2	0.67	23.00	652	66963	FW

Table 6. Results of parametric study on the effect of face thickness and core density (t_c = 150mm, L = 3m)

Face Thickness (mm)	**Core Density = 80 kg/m^3**							**Core Density = 200 kg/m^3**							**Core Density = 320 kg/m^3**						
	Initial Stiffness, K (N/mm)	Ultimate Stiffness, K_u (N/mm)	$\frac{K_u}{K_i}$	Peak Load, P_u (kN)	Def. at Peak, δ_u (mm)	Facing Strain at Peak, ε_u (μ ε)	Failure Mode	Initial Stiffness, K (N/mm)	Ultimate Stiffness, K_u (N/mm)	$\frac{K_u}{K_i}$	Peak Load, P_u (kN)	Def. at Peak, δ_u (mm)	Facing Strain at Peak, ε_u (μ ε)	Failure Mode	Initial Stiffness, K (N/mm)	Ultimate Stiffness, K_u (N/mm)	$\frac{K_u}{K_i}$	Peak Load, P_u (kN)	Def. at Peak, δ_u (mm)	Facing Strain at Peak, ε_u (μ ε)	Failure Mode
3	36.8	25.2	0.69	4.09	162	15250	FW	40.5	27.4	0.67	7.78	405	40909	FW	41.1	27.7	0.67	11.28	654	66947	FW
6	68.3	26.9	0.39	8.34	310	15282	FW	82.5	56.1	0.68	15.85	409	40870	FW	84.7	57.2	0.67	23.00	652	66963	FW
9	95.4	24.4	0.25	12.75	522	15264	FW	125.7	85.9	0.68	24.23	415	40884	FW	130.9	88.5	0.67	35.15	653	66954	FW
12	118.9	25.0	0.21	15.25	609	12494	CS	170.0	124.9	0.73	37.63	517	49142	FW	179.6	130.9	0.72	47.70	664	66958	FW

Table 7. Results of parametric study on the effect of span length and core density (t_f = 6mm, t_c = 150mm)

Span Length (m)	**Core Density = 80 kg/m^3**							**Core Density = 200 kg/m^3**							**Core Density = 320 kg/m^3**						
	Initial Stiffness, K (N/mm)	Ultimate Stiffness, K_u (N/mm)	$\frac{K_u}{K_i}$	Peak Load, P_u (kN)	Def. at Peak, δ_u (mm)	Facing Strain at Peak, ε_u (μ ε)	Failure Mode	Initial Stiffness, K (N/mm)	Ultimate Stiffness, K_u (N/mm)	$\frac{K_u}{K_i}$	Peak Load, P_u (kN)	Def. at Peak, δ_u (mm)	Facing Strain at Peak, ε_u (μ ε)	Failure Mode	Initial Stiffness, K (N/mm)	Ultimate Stiffness, K_u (N/mm)	$\frac{K_u}{K_i}$	Peak Load, P_u (kN)	Def. at Peak, δ_u (mm)	Facing Strain at Peak, ε_u (μ ε)	Failure Mode
3	68.3	26.9	0.39	8.34	310	13580	FW/CS	82.5	56.1	0.68	15.85	438	40870	FW	84.7	57.2	0.67	23.00	683	66963	FW
4	32.7	20.1	0.61	6.26	311	15276	FW	35.6	24.1	0.67	11.89	735	40884	FW	36.0	24.2	0.67	17.25	1168	66963	FW
5	17.3	9.2	0.53	5.01	544	15287	FW	18.3	12.3	0.67	9.51	1119	40870	FW	18.5	12.4	0.67	13.80	1799	66963	FW
6	10.4	7.0	0.70	4.17	594	15258	FW	10.7	7.2	0.67	7.93	1592	40905	FW	10.7	7.2	0.67	11.50	2572	66963	FW

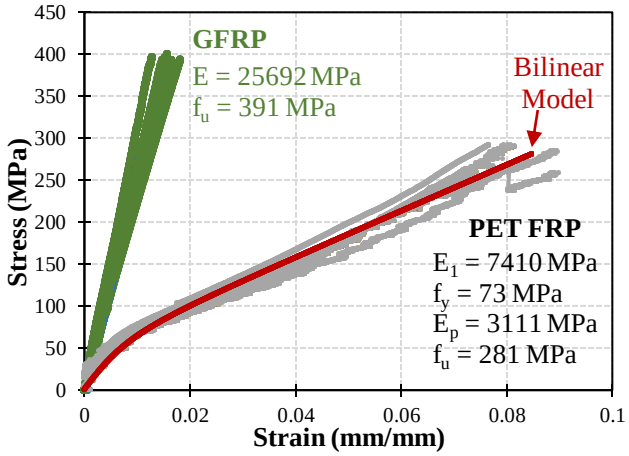

Figure 1. Experimental and computed stress-strain curves of facing materials.

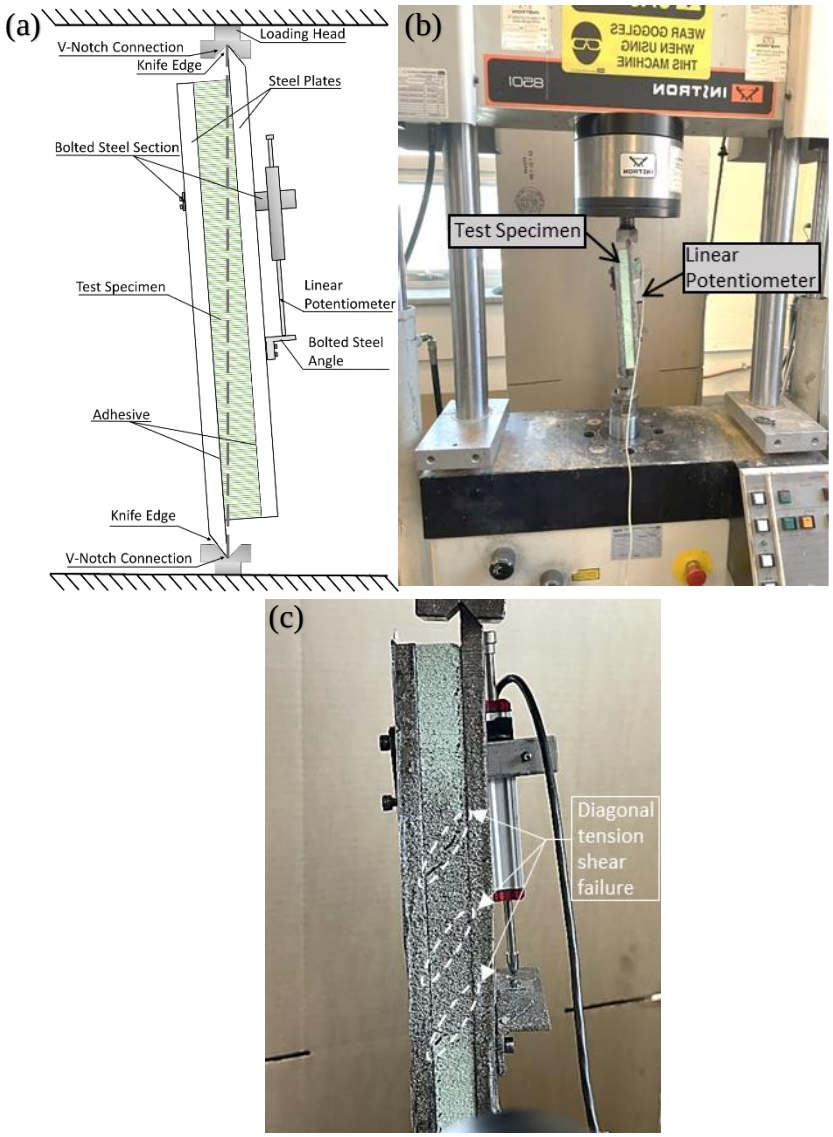

Figure 2. Core shear testing set-up and instrumentation: (a) annotated sketch of the core shear test; (b) core specimen set on Instron 8501 for the shear test; (c) R-PET foam core post shear failure.

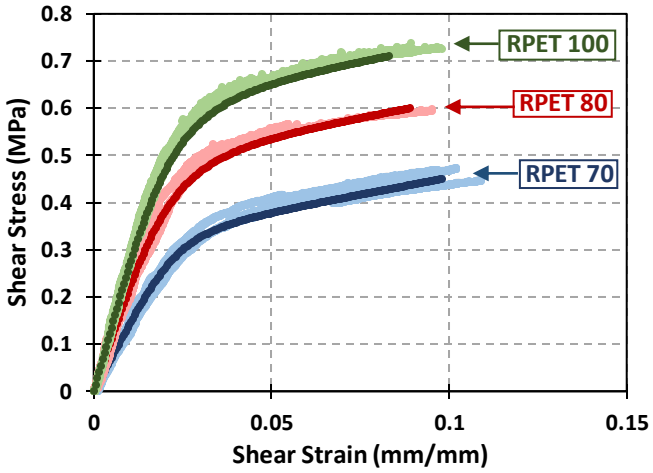

Figure 3. Experimentally derived shear stress-strain of R-PET core component (darker curves are the proposed non-linear model).

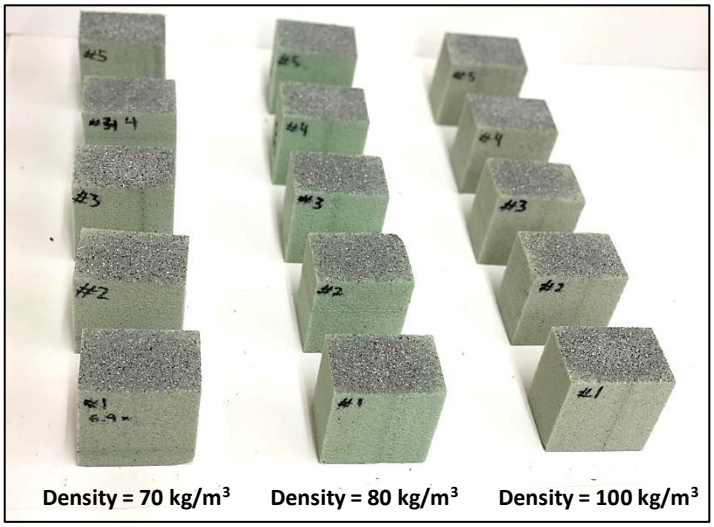

Figure 4. Cuboidal specimens of R-PET foam with relative densities of 70 kg/m^3, 80 kg/m^3, and 100 kg/m^3 prepared for compression testing.

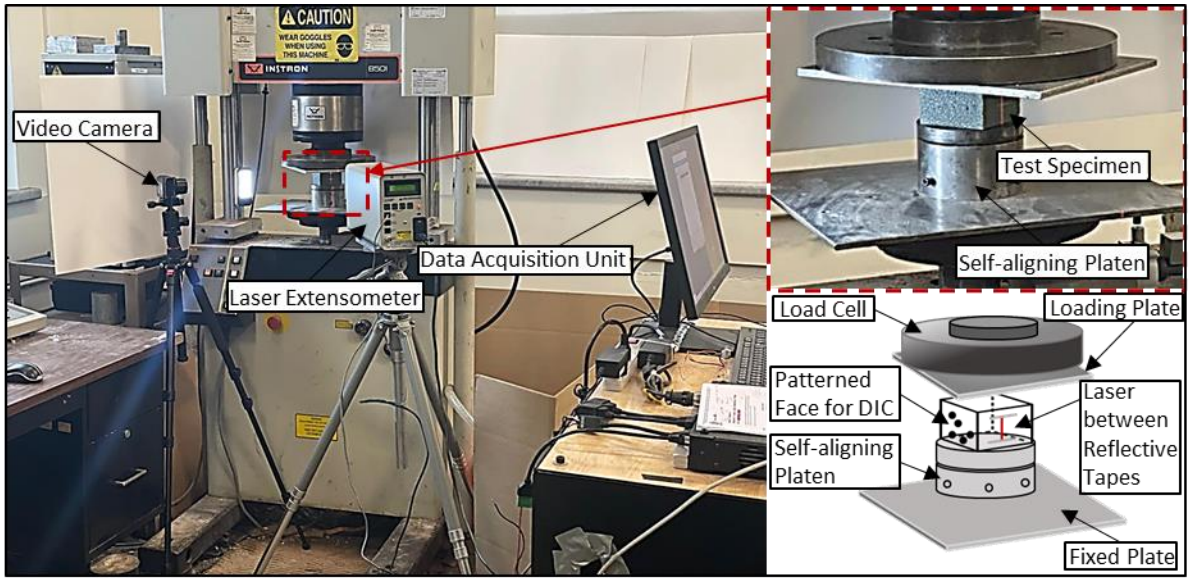

Figure 5. Annotated compression testing set-up of R-PET foam specimen.

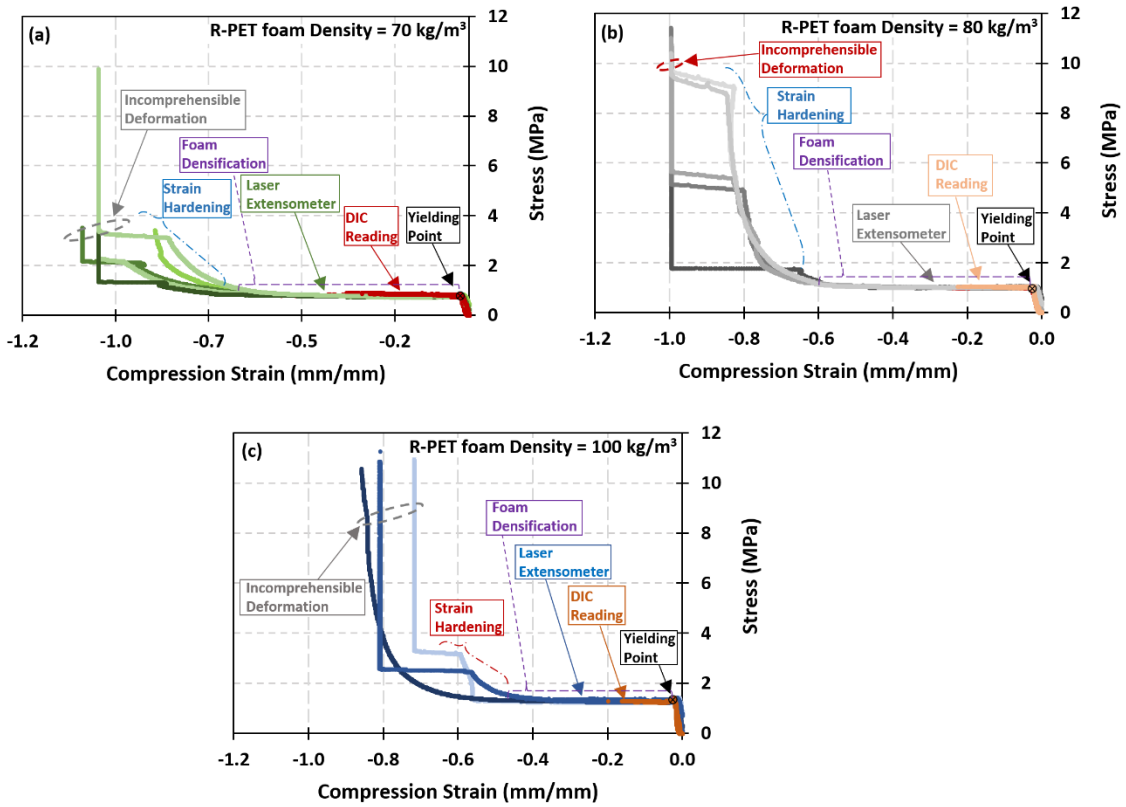

Figure 6. Stress vs strain curves of R-PET sets with a density of: (a) 70 kg/m^3, 80 kg/m^3, (b) 100 kg/m^3.

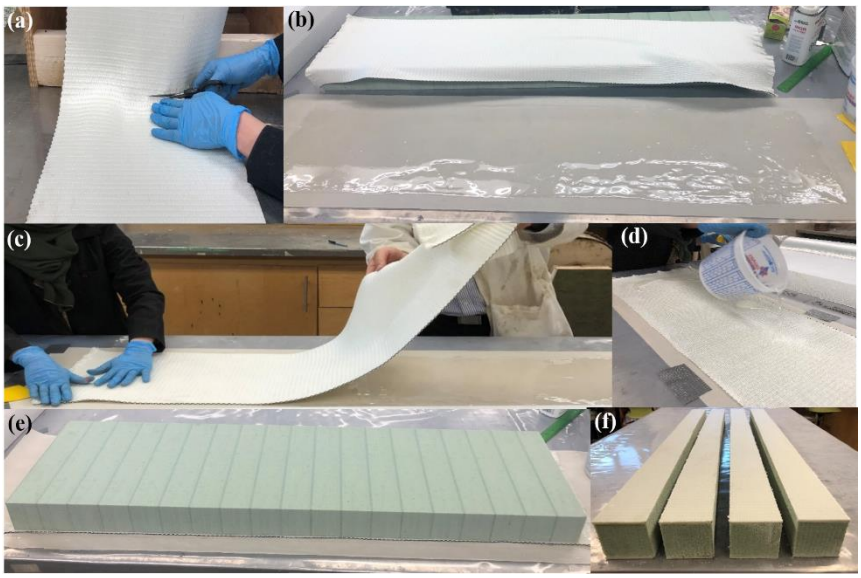

Figure 7. Fabrication process of sandwich panels: (a) fabric layer cut to the required length; (b) epoxy and hardener spread on parchment paper (c) unidirectional fabric placed on a layer of resin; (d) another layer of resin spread on fabric layer; (e) core component, with a 1200mm length 300mm width and 76mm thickness, placed on top of epoxy layer; (f) sandwich panel cut into four sections.

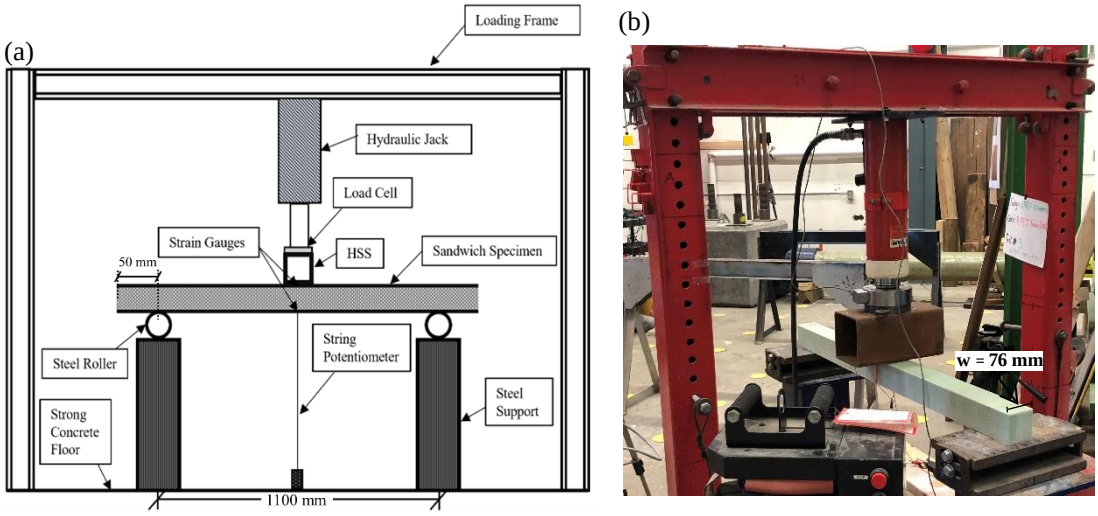

Figure 8. Experimental test set-up of three-point bending test: (a) schematic illustration of the set-up; and (b) photo of the beam specimen during testing.

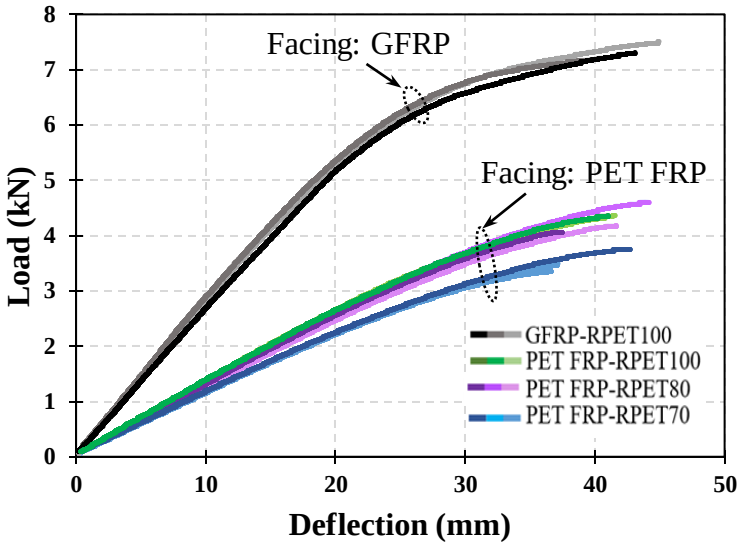

Figure 9. Load vs deflection curve of sandwich panels under three-point bending.

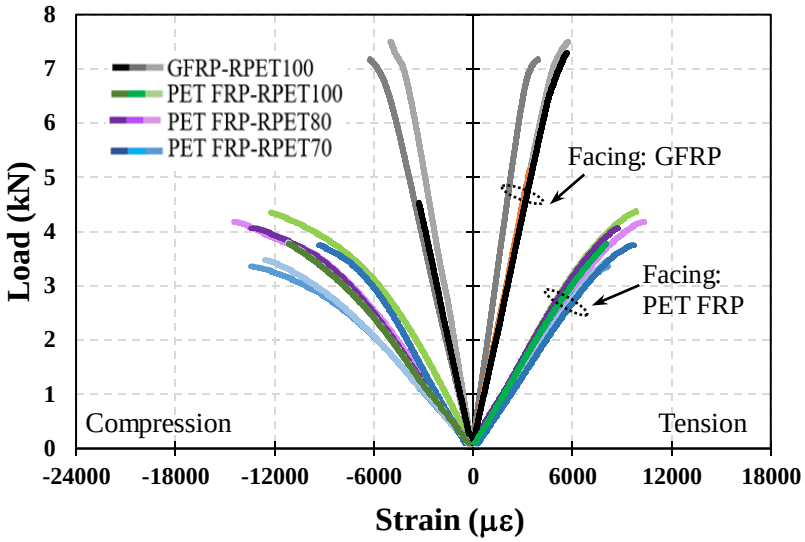

Figure 10. Compression and tension strain with respect to the applied load of the tested sandwich panels.

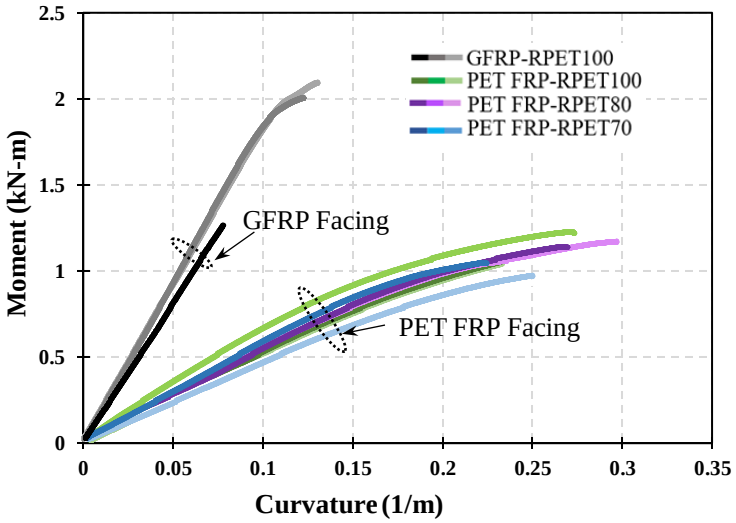

Figure 11. Moment vs curvature diagram associated with all the sandwich panel sets.

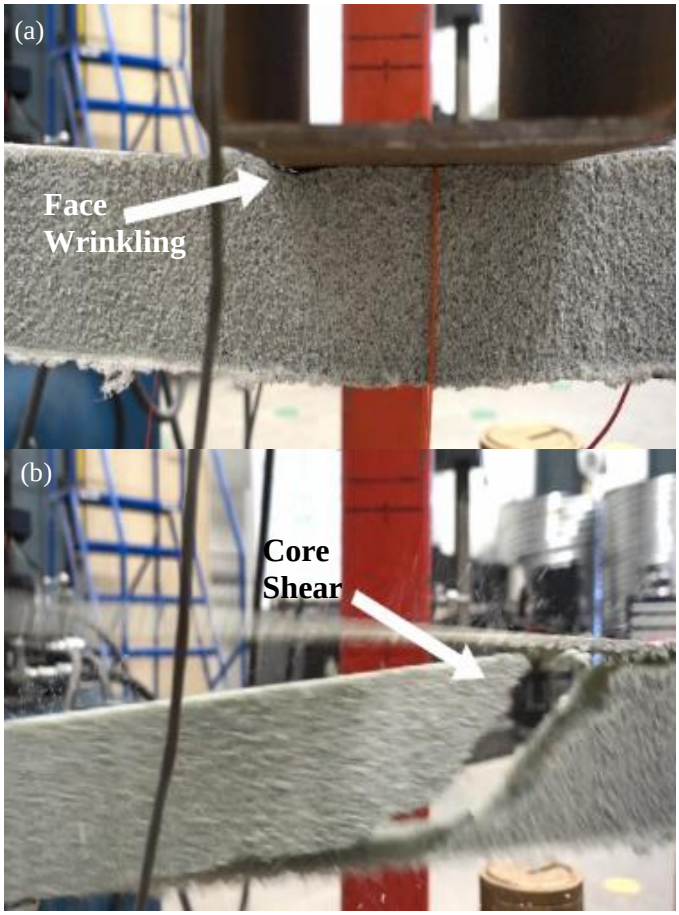

Figure 12. Side-view of the beam showing the sequence at which it failed. (a) Wrinkling of the top face appears, and (b) core fails in shear.

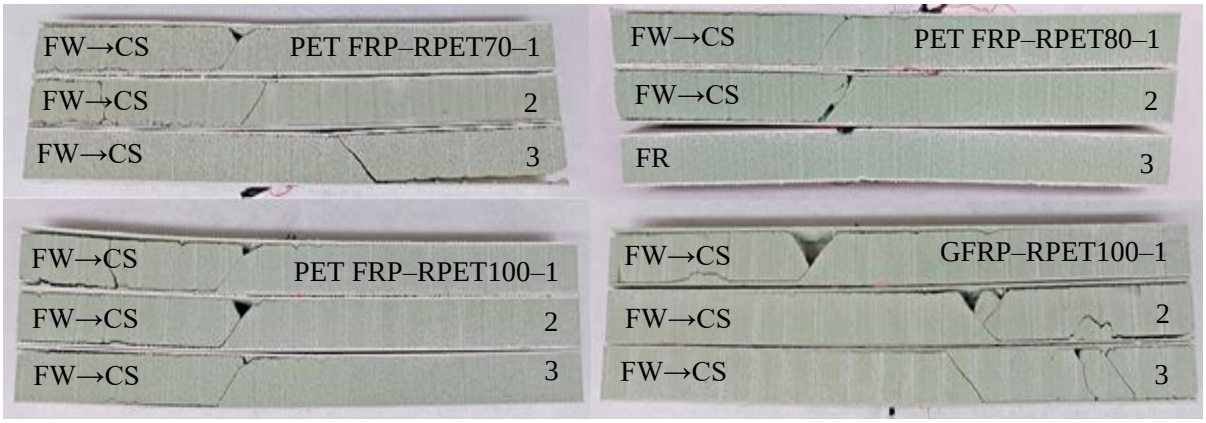

Figure 13. Side-view images of tested beams

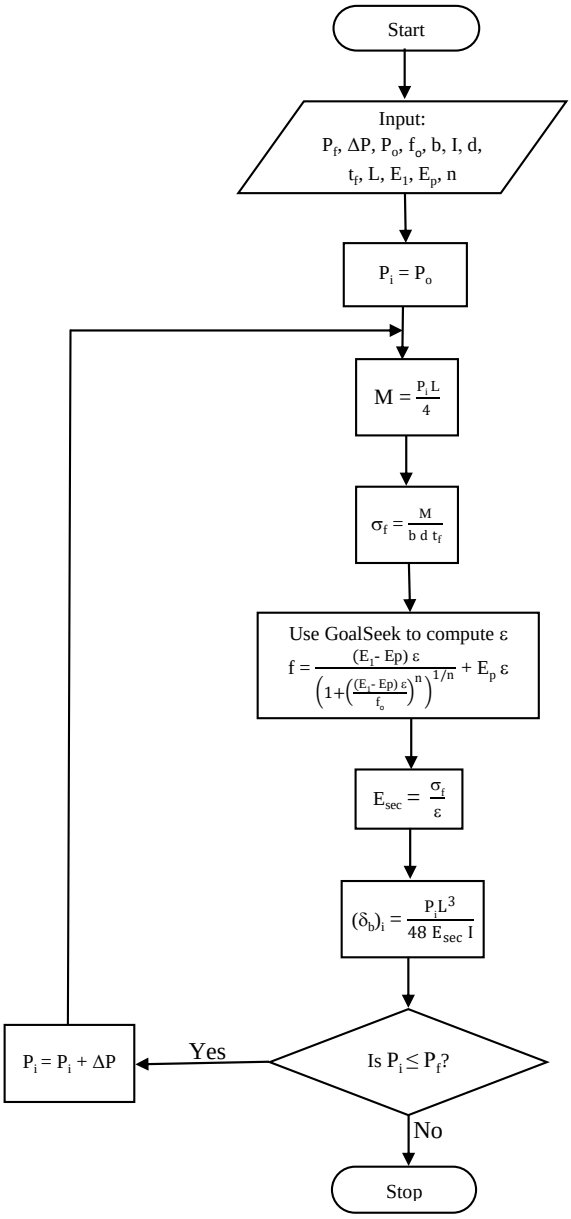

Figure 14. Flowchart of iterative procedure computing non-linear bending deformation

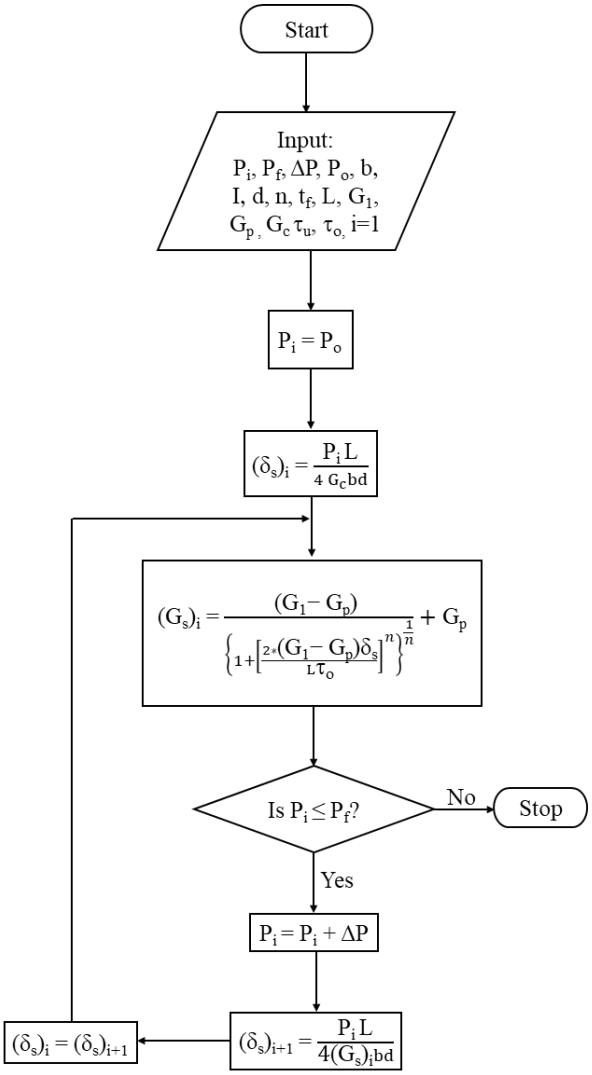

Figure 15. Flowchart of iterative procedure computing non-linear shear deformation.

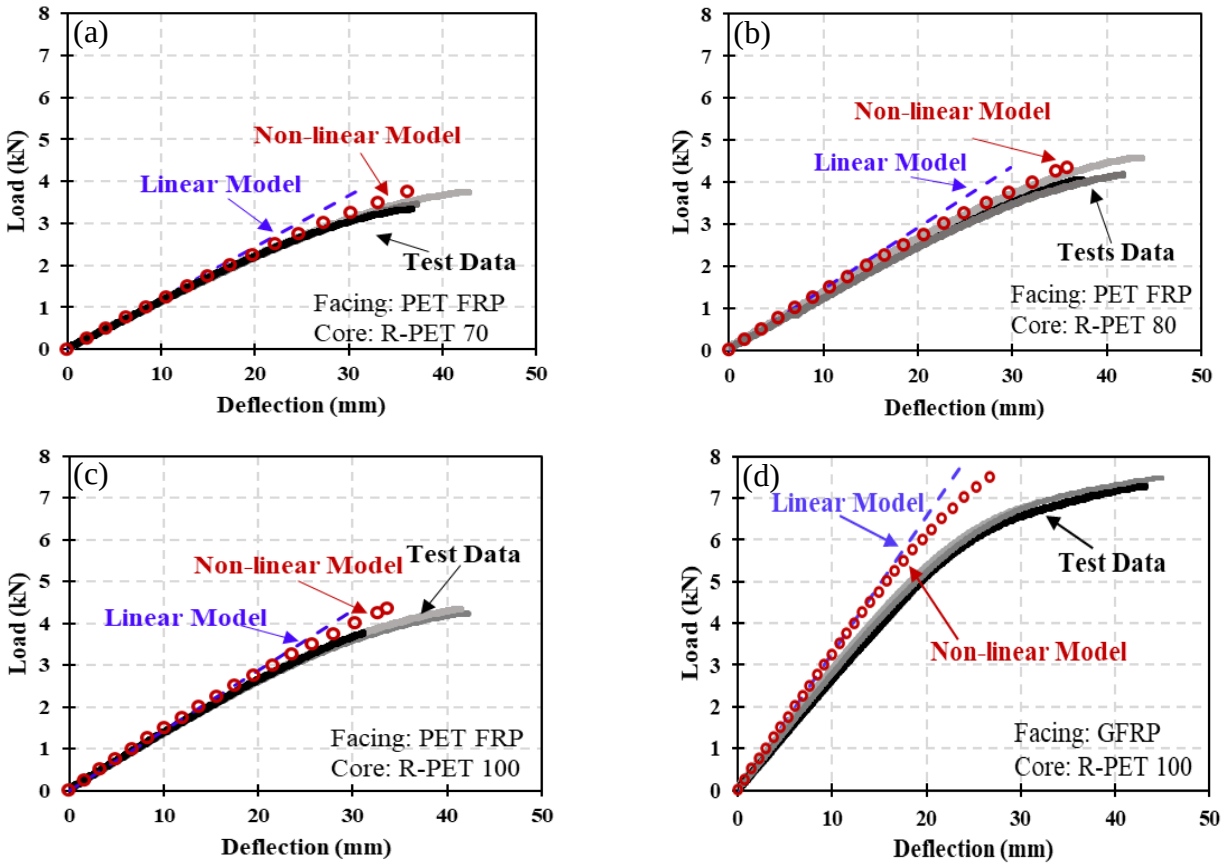

Figure 16. Load vs midspan deflection curves of sandwich panel sets made from (a) PET FRP facing and R-PET 70 foam core, (b) PET FRP facing and R-PET 80 foam core, and (c) PET FRP facing and R-PET 100 foam core, (d) GFRP facing and R-PET 100 foam core under three-point bending.

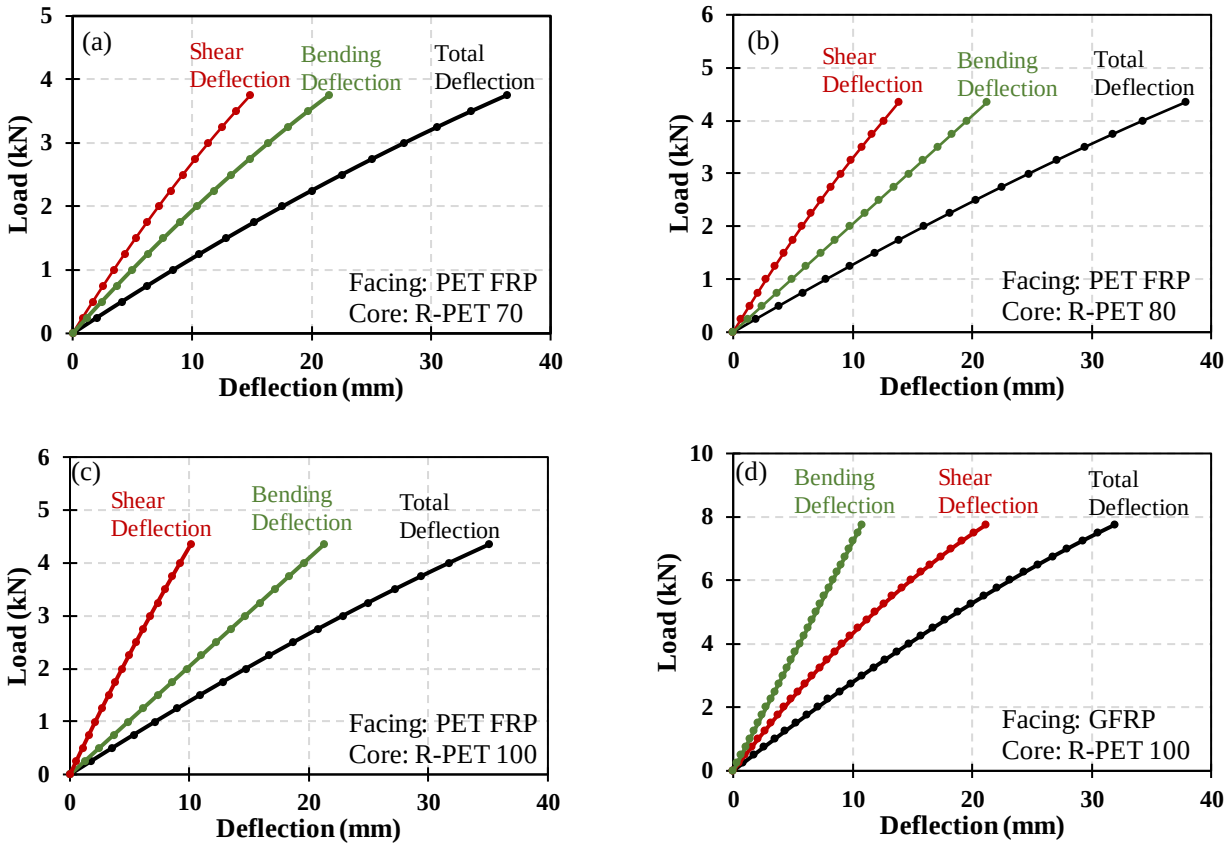

Figure 17. Breakdown of total midspan deflection into shear and bending deflections of the modeled sandwich beams: (a) PET FRP-R-PET 70, (b) PET FRP-R-PET 80, PET FRP-R-PET 100, GFRP-R-PET 100.

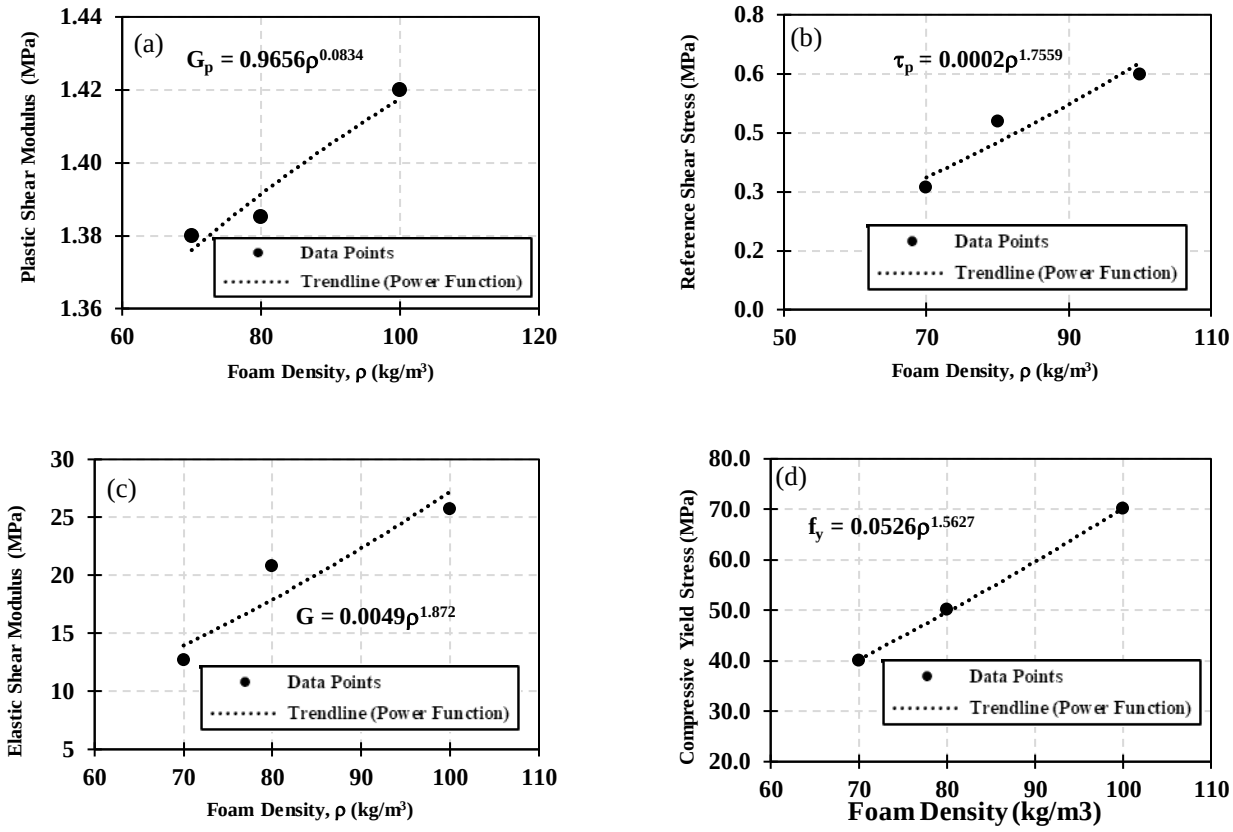

Figure 18. Change in mechanical properties with respect to core density: (a) plastic shear modulus vs foam density; (b) reference shear stress vs foam density; (c) elastic shear modulus vs foam density; (d) compressive yield stress vs foam density.

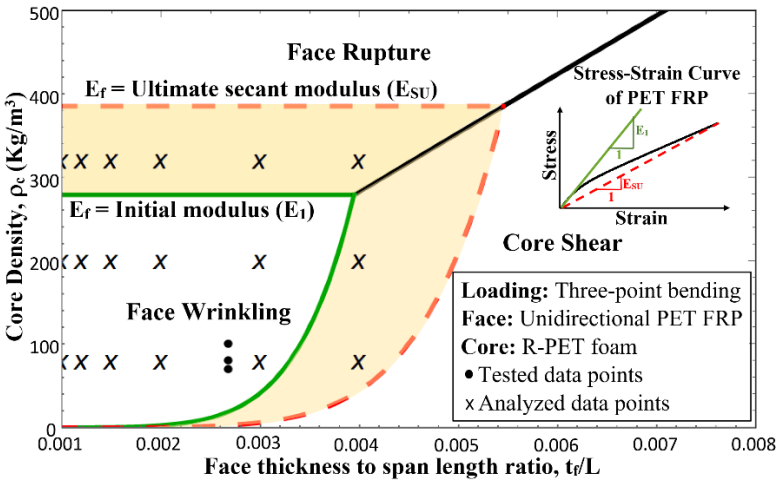

Figure 19. Failure mode map of PET FRP-R-PET sandwich panel under three-point bending.

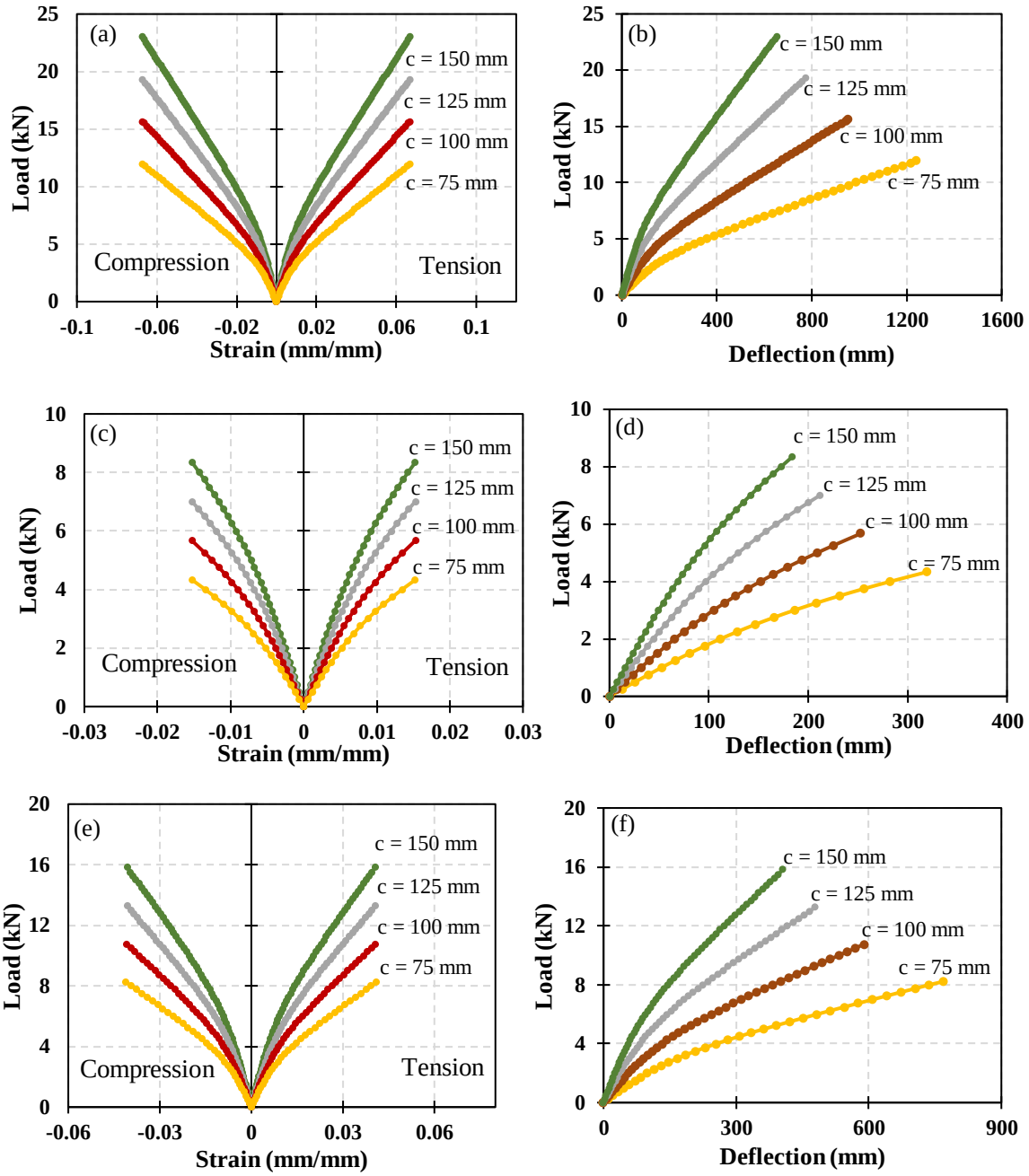

Figure 20. Stress-strain and load-deflection curves for sandwich panels with varying core thickness and core density; (a-b) density = 80 kg/m3, (c-d) density = 200 kg/ m3, (e-f) density = 320 kg/ m^3.

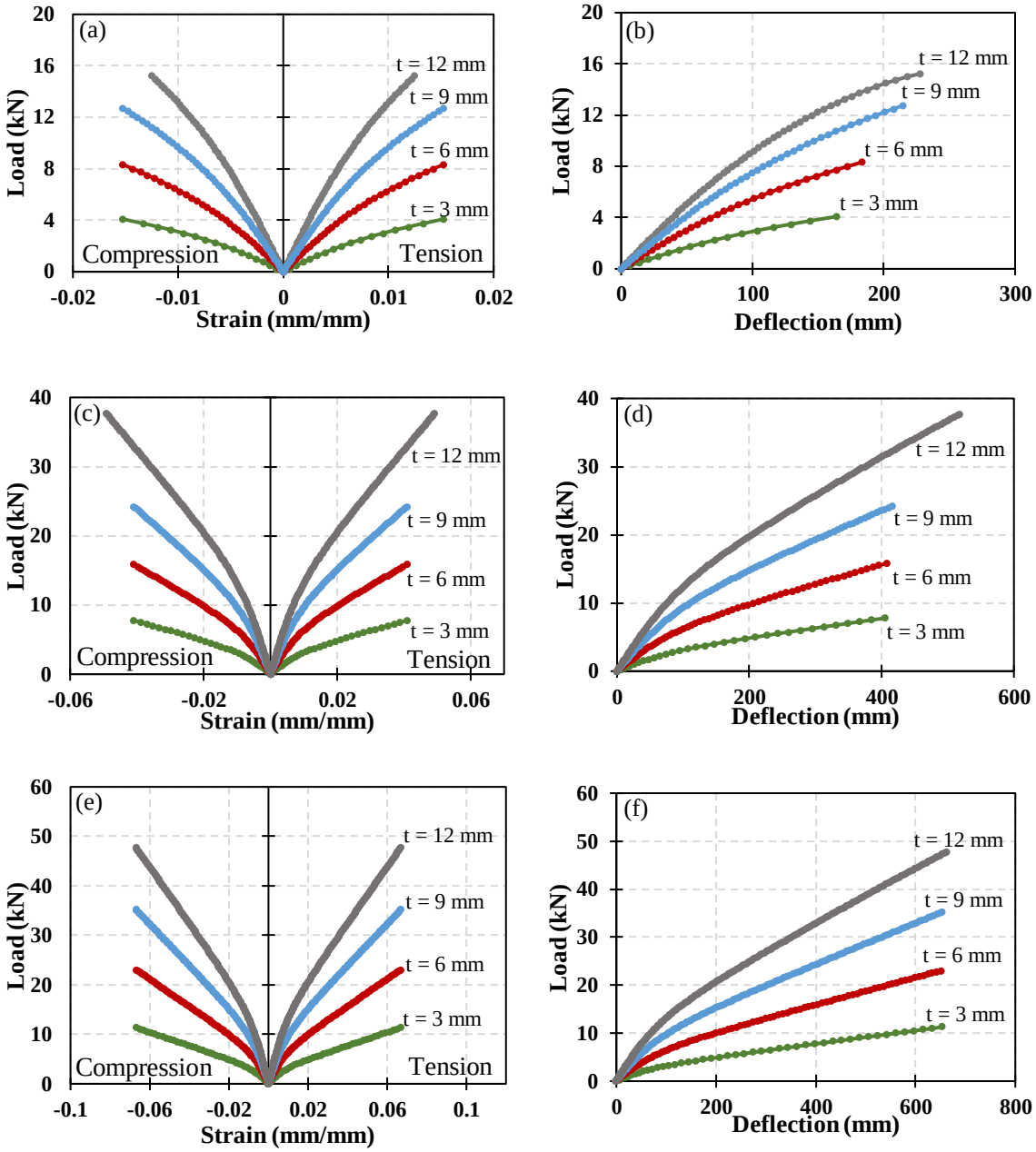

Figure 21. Stress-strain and load-deflection curves for sandwich panels with varying facing thickness and core density; (a-b) density = 80 kg/m^3, (c-d) density = 200 kg/ m^3, (e-f) density = 320 kg/ m^3.

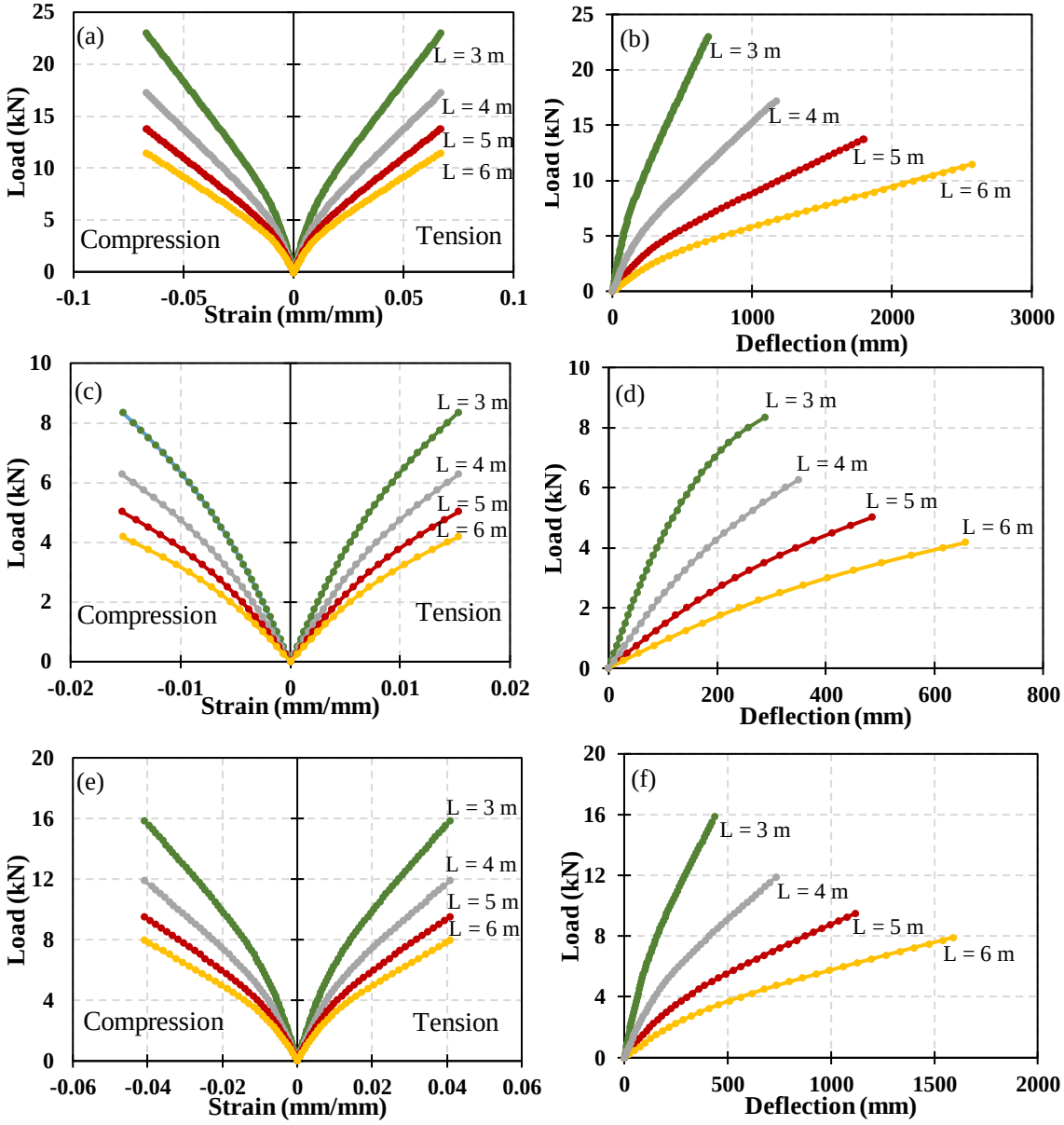

Figure 22. Stress-strain and load-deflection curves for sandwich panels with varying span length and core density; (a-b) density = 80 kg/m^3, (c-d) density = 200 kg/ m^3, (e-f) density = 320 kg/ m^3.